Diplomarbeit

Self-Consistent Ornstein-Zernike Approximation for Simple Fluids and Their Mixtures

Ausgeführt am Institut für
Analysis und Scientific Computing
der Technischen Universität Wien

unter der Anleitung von Ao.Univ.Prof. Dipl.-Ing. Dr.techn. Dr.rer.nat.
Frank Rattay
durch

Dipl.-Ing. Dr.techn. Elisabeth Schöll-Paschinger
Bürgerspitalgasse 29/24, 1060 Wien

Wien, am 29. März 2004 _____

Zusammenfassung

Phasenübergänge in Flüssigkeiten sind vertraute Vorgänge aus unserem Alltagsleben, und ihre theoretische Beschreibung trägt wesentlich zu einem tieferen Verständnis dieser komplexen Phänomene bei. In dieser Arbeit haben wir, um die Abhängigkeit des Phasenverhaltens einer Substanz von ihren mikroskopischen Eigenschaften zu untersuchen, zur Weiterentwicklung klassischer Flüssigkeitstheorien beigetragen und diese auf einfache Flüssigkeiten sowie deren Mischungen angewandt. Der von uns verwendete theoretische Zugang ist die *Self-Consistent Ornstein-Zernike Approximation* (SCOZA), eine mikroskopische Flüssigkeitstheorie, die sehr genaue Resultate für die Koexistenzkurve liefert und deren Vorhersagen sogar im kritischen Bereich des Phasendiagramms präzise bleiben. Diese Theorie wurde von uns für eine Flüssigkeit von sphärischen Teilchen erweitert, deren Paarwechselwirkung sich aus einem Hartkugelanteil und einer Linearkombination von Sogami-Ise Potentialen zusammensetzt. Die Vorhersagen für thermodynamische Größen, das Phasenverhalten und den kritischen Punkt wurden mit Resultaten der *Optimized Random Phase Approximation* (ORPA) - einer inkonsistenten mikroskopischen Flüssigkeitstheorie - verglichen, um den Einfluß der thermodynamischen Konsistenzbeziehung zu untersuchen. Weiters haben wir uns mit zweikomponentigen Flüssigkeitsmischungen beschäftigt, die im Vergleich zu Einkomponentenflüssigkeiten ein wesentlich reicheres Phasenverhalten aufweisen. Wir haben die SCOZA für eine sogenannte symmetrische binäre Flüssigkeit erweitert. Drei Typen von Phasendiagrammen, die durch den Ort charakterisiert werden, wo die λ-Linie (die kritische Linie von Entmischungübergängen) die Flüssig-Gas Koexistenzkurve schneidet, konnten identifiziert werden, und lieferten eine quantitative Ergänzung zu Untersuchungen mit einer Mean Field Theorie. Insbesondere haben wir den Einfluß der Reichweite der Wechselwirkungen auf das Phasenverhalten untersucht und Phasendiagramme von Systemen mit langreichweitigen Wechselwirkungspotentialen berechnet.

Abstract

Phase transitions in fluids are practically ubiquitous in our everyday lives and their theoretical description is essential for a deeper understanding of these complex phenomena. In an effort to gain more insight into the relationship between the microscopic properties of a fluid and its phase behavior we have contributed to a further development of classical liquid-state theories and have applied them to simple fluids and their mixtures. In particular, we have focused on the *Self-Consistent Ornstein-Zernike Approximation* (SCOZA), a microscopic liquid-state theory that is known to give highly accurate results for the coexistence curves and that remains successful even in the critical region. We have generalized the SCOZA to a fluid of spherical particles with a pair potential given by a hard-core repulsion and a linear combination of Sogami-Ise tails, i.e. a sum of a Coulomb and constant potential that are both exponentially damped. The predictions for the thermodynamics, the phase behavior and the critical point are compared with results from the Optimized Random Phase Approximation (ORPA) and the effect of thermodynamic consistency is investigated. Further work is dedicated to binary fluid mixtures: their phase behavior shows, compared to simple one-component fluids, a much richer variety of phenomena. We have extended the SCOZA to the case of a symmetric binary mixture: here the like-particle interactions are equal, while the interactions between the unlike fluid particles differ from the like ones. Three archetypes of phase diagrams, characterized by the location where the λ-line (i.e. the critical line of demixing transitions) intersects the vapor-liquid coexistence curve were identified, supplementing thus previous mean-field type studies in a quantitative way. In addition, we study the influence of the interaction range on the phase behavior and present phase diagrams of binary symmetric systems with very long-ranged interactions that are close to Coulomb interactions.

Contents

Chapter 1

Introduction

Phase transitions are practically ubiquitous in our everyday lives, ranging from very simple, commonplace events to rather complicated and sophisticated production processes in industry where special knowledge of the phase diagrams of substances is required. Therefore, the technological aspect of investigations in phase diagrams is of importance and industrial developments and processes often rely on accurate and reliable phase diagrams.

Phase transitions belong to the most challenging and fascinating problems in physics. The complexity of these phenomena, their large diversity (such as transitions from liquid to gas, from the conducting to the superconducting phase, from a paramagnet to a ferromagnet, demixing separations in mixtures and others), and the discovery of new phases (such as quasi-crystals or superfluids) has attracted the interest of condensed matter scientists in this research field. One of the central challenging questions is: How do the microscopic properties of a system influence its phase behavior and its critical phenomena? During the past decades significant contributions to describe phase transitions have been proposed in theoretical and computational physics. Meanwhile, theoretical concepts in combinations with computational tools can be considered as complements to experimental techniques: on the one side they are able to reproduce experimental results with high accuracy and contribute thus to a deeper insight into these phenomena; on the other side they might be more economical than experiments and are able to indicate, whether it is worthwhile to push experiments in a direction where difficult experimental conditions are to be expected. They can sometimes even predict results which are barely accessible in experiment (such as matter under extreme conditions).

The discontinuities in physical behavior, which occur when a system undergoes a phase transition, have claimed the attention of scientists for many years. It was recognized already in the 19th century that the discontinuities are associated with the in-

teractions between the microscopic particles of the system. Thus it became necessary to develop a statistical mechanical treatment of phase transitions [1]. The first steps in this direction were done in the fundamental works of van der Waals and Weiss who explained phase transitions in fluid and magnetic systems with mean field theories. Further progress was achieved by Landau in his phenomenological explanations which provide insight into the detailed character of the discontinuities. In 1944 the modern era in phase transitions started when Onsager found an exact statistical mechanical solution for the two-dimensional Ising model. His solution showed that previous 'classical' theories were unreliable in their quantitative predictions and stimulated a closer investigation of the true behavior near discontinuities.

Particular interest has been focused on phenomena associated with critical points such as that of gas-liquid equilibrium, or the Curie point in ferromagnetic materials. In the critical region, anomalies in thermodynamic functions are observed which result in the divergence of such thermodynamic quantities as specific heat, compressibility, etc. These critical fluctuations are very difficult to handle theoretically and much effort has gone into this. Starting in the 1960's considerable progress towards a greater understanding of critical phenomena was made by introducing the ideas of renormalization group theory [2].

In the present work we intend to contribute to a deeper understanding of phase transitions. Various concepts were proposed over the last decades to describe these phenomena from a theoretical point of view: One of them is the above mentioned renormalization group theory which is the most successful tool to study cooperative phenomena in statistical mechanics and has lead to a deeper understanding of phase transitions and critical phenomena. However, it it not able to predict non-universal quantities (such as the location of the critical point). Computer simulations represent another access to the problem [3]. For a given interparticle potential they provide 'quasi' exact results – apart from finite size effects induced by the finite size of the simulation cell. These effects become obviously more severe in the critical regions where long-range fluctuations occur. Sophisticated techniques are meanwhile available to cope with this problem. In this work we have chosen another theoretical approach, namely microscopic liquid-state theories that are based on statistical mechanics [4]. The aim of these theories is to predict the thermodynamic and structural properties of a fluid from the presumed knowledge of the forces between the fluid particles. So once the interparticle forces are fixed, the theory should be able to determine the phase behavior (including criticality) of the system.

In this work we have focused on the phase behavior of fluids. Over the past decade much evidence was found that the fluid states, gas and liquid, possess many structural similarities and that both are quite distinct from the solid state. Hence, it is not surprising

that the same theoretical approach can be used to describe both the liquid, the gas and the supercritical fluid. In this work we will be exclusively concerned with the phase behavior of fluids and their mixtures, i.e. we restrict our investigations to that part of the entire phase diagram that includes liquid-gas transitions and liquid-liquid demixing transitions in mixtures omitting the determination of the melting line that would require in addition other theoretical approaches like e.g. classical density functional theory.

Apart from the one-component fluid we also study the properties of fluid mixtures; here new phenomena are encountered that are not present in pure substances. According to the Gibbs rule now up to four phases can be observed simultaneously and the way these phases can coexist often leads to rather complex phase diagrams. The phase behavior is mainly triggered by two mechanisms (and their interrelation): first, there is the size difference of the particles of the two components and their (partial) penetrability; second, there is the chemical influence, expressed via the set of the three interatomic potentials. Depending on the relative sizes of the particle species and the properties of the interaction forces a large variety of different types of phase behavior can be observed [5].

We shall exclusively consider simple classical liquids with interparticle potentials, that can be considered as realistic models of a fairly large number of real fluids. 'Quasi-experimental' data for these systems are available from computer simulations (either Monte Carlo or Molecular Dynamics simulations). Comparison of these data with those from sophisticated microscopic liquid-state theories has shown that these theories produce results for systems well inside the liquid-state region that are practically indistinguishable from the simulation data. However, the accuracy of these approaches begins to decrease as one leaves the liquid-state region and approaches the liquid-gas coexistence curve and/or the critical region. In particular, the shape of the coexistence curve and the location of the critical point is not reproduced correctly and the critical exponents are not the exact ones. Some theoretical approaches even fail to converge in the critical region, so that the liquid and vapor branches of the coexistence curve remain unconnected. To overcome this highly unsatisfactory situation two microscopic liquid-state theories have been developed in the past years that cope with the problems encountered in the critical region and near the phase boundaries: one is the self-consistent Ornstein Zernike approximation (SCOZA) [6], the other one is the hierarchical reference theory (HRT) [7] that merges concepts of renormalization group theory with liquid-state theories.

This work is dedicated to the SCOZA which was proposed by Stell and Høye already in the 1970s; the OZ relation is supplemented with a generalized mean spherical ansatz (GMSA), introducing in the MSA relation a density- and temperature-dependent function which is determined by enforcing consistency between the different thermodynamic routes.

Although introduced nearly thirty years ago its first numerical implementation was - due to substantial numerical problems - successfully realized only a few years ago in 1996 [8]: a reformulation of the SCOZA partial differential equation made an access to subcritical temperatures possible. Ever since, the SCOZA has been applied only to a few discrete and continuum systems restricted in the latter case to hard-core Yukawa systems. However, these results showed in an impressive way that this theory remains successful even in the critical region: it is able to predict critical temperatures within 0.6% (or even less) and to reproduce the exact value for the critical exponent β very accurately.

The obvious success of the SCOZA has motivated us to contribute to its extension: further development of the SCOZA and its application to a larger variety of systems are summarized in this work. In the case of continuum fluids the SCOZA has been solved up to now only for hard-core Yukawa systems. This restriction can be traced back to the fact that the SCOZA is based on the semi-analytic MSA solution which is available for multi-component hard-core multi-Yukawa systems. In this work we have generalized the SCOZA to one-component fluids with hard-core multi-Sogami-Ise interactions. This modification increases the variety of systems that can now be studied: any smooth realistic interaction can be modeled by a suitable linear combination of Sogami-Ise tails.

Furthermore, we have generalized the SCOZA to a binary symmetric hard-core Yukawa mixture: here the interaction between like particles is equal, only the interaction between the different particle species is different; phase diagrams were calculated for various system parameters. Despite its simplicity this model system shows a very rich variety of phase behavior and interesting phenomena can be observed such as a critical end point or a tricritical point that is not present in a general binary mixture. Three different types of phase diagrams can be distinguished, classified by the location where the λ-line (the critical line of the demixing transitions) intersects the first order vapor-liquid coexistence curve. As already shown in a qualitative mean field study [9] the sequence of these types of phase diagrams is triggered by a microscopic parameter, i.e., the interaction ratio of the unlike to the like interactions. In contrast to conventional liquid-state theories we are able to obtain results even in the critical regions. In addition, we have studied the influence of the interaction range on the phase behavior; results have also been obtained for the case of very long-ranged Yukawa interactions, i.e. interactions that are close to Coulomb interactions.

This work is organized as follows: in the first part we summarize in sect. 2.1 briefly the statistical mechanics foundations of microscopic liquid-state theories, we define the structure functions and their relationships with thermodynamic quantities. In sect. 2.2 we give a brief overview over two classes of microscopic liquid-state theories: integral

equation theories and perturbation theories and discuss especially those approximations that are related to this work: the MSA and the Lowest-Order γ-ordered Approximation (LOGA) or the equivalent Optimized Random Phase Approximation (ORPA). In chapter 3 basic thermodynamic concepts and quantities necessary to describe phase equilibria and stability conditions are introduced and the different types of phase diagrams that occur in a binary symmetric fluid are schematically illustrated.

The second part is dedicated to the SCOZA: in sect. 4.1 we first give an overview over thermodynamically self-consistent liquid-state theories putting emphasize on the presentation of the SCOZA; In sect. 4.2 we then formulate the SCOZA for a one-component hard-core multi-Sogami-Ise fluid and present results for various model systems. The SCOZA for a binary symmetric fluid is formulated in sect. 4.5 where also results are presented.

Chapter 2

Theoretical Concepts

The aim of statistical mechanics is to provide a macroscopic description of a system based on its microscopic properties. Starting with a given interparticle law of force of a certain fluid model one should be able to derive its structural and thermodynamic properties and to determine the type of phase equilibria that will be encountered in the system.

The central quantity in liquid-state theory that provides the link between the microphysics and macrophysics of a fluid is the so called pair distribution function $g(r)$. It measures the degree of correlation between the particles separated by a distance r and thus describes the structure of a fluid. In fact, basic thermodynamic quantities as the pressure or the internal energy from which all other thermodynamic quantities, relevant for the determination of phase coexistence, can be determined, are expressible in terms of this function. On the other hand, the pair distribution function itself is a functional of the interparticle potential. However, to calculate $g(r)$ for a given interaction potential is a complex and unsolvable problem and some simplifying assumption must be made for an approximate determination of the pair distribution function and hence of the structure. These approximation schemes include on the one hand integral equation theories (IETs) where an integral equation, in which $g(r)$ is the unknown function, has to be solved. Another group of approximation schemes are the perturbation theories, which represent generalizations of the theory of van der Waals and calculate thermodynamic and structural properties as perturbation to those of the well known hard-sphere reference system.

In the following chapter we will first briefly introduce some basic definitions of the structural functions and their relationships with thermodynamic quantities; then some approximation schemes of liquid-state theory will be presented. Emphasis will be put on those concepts that are used in the present work: the mean spherical approxima-

tion (MSA) and the Lowest-Order γ-ordered Approximation (LOGA) or the equivalent Optimized Random Phase Approximation (ORPA).

2.1 Structure functions

2.1.1 Radial distribution function

We define the structure functions in the canonical ensemble. So we consider a macroscopic system of N identical particles, enclosed in a volume V at a given temperature T. The potential energy of the system is assumed to be given by $V_N(\mathbf{r}^N)$, where we use the notation $\mathbf{r}^N = \{\mathbf{r}_1, \mathbf{r}_2, \ldots, \mathbf{r}_N\}$ for the positions of the N particles.

Then the one-particle density, that is defined as the ensemble average over the local particle density

$$\rho(\mathbf{r}) = \sum_{i=1}^{N} \delta(\mathbf{r} - \mathbf{r}_i) \tag{2.1}$$

is

$$\rho_N^{(1)}(\mathbf{r}) = \left\langle \sum_{i=1}^{N} \delta(\mathbf{r} - \mathbf{r}_i) \right\rangle = \frac{N}{Q_N(V,T)} \int \ldots \int e^{-\beta V_N(\mathbf{r}, \mathbf{r}_2, \ldots, \mathbf{r}_N)} d^3r_2 \ldots d^3r_N, \tag{2.2}$$

where $\beta = 1/k_B T$ is the inverse temperature, k_B the Boltzmann constant, and

$$Q_N(V,T) = \int e^{-\beta V_N(\mathbf{r}^N)} d^3r_1 \ldots d^3r_N \tag{2.3}$$

the configurational integral. For a homogenous system it follows that $\rho^{(1)}(\mathbf{r}) = \frac{N}{V} = \rho$.

Similarly, the probability of finding any two particles in the volume elements d^3r_1 and d^3r_2 at $\mathbf{r}_1$ and $\mathbf{r}_2$, irrespective of the positions of the other particles, is given by [10, 4]

$$\rho_N^{(2)}(\mathbf{r}_1, \mathbf{r}_2) d^3r_1 d^3r_2 = \frac{N(N-1)}{Q_N(V,T)} \left[\int \ldots \int e^{-\beta V_N(\mathbf{r}^N)} d^3r_3 \ldots d^3r_N \right] d^3r_1 d^3r_2, \tag{2.4}$$

where $\rho_N^{(2)}(\mathbf{r}_1, \mathbf{r}_2)$ is called the two-particle density. The factor $N(N-1)$ takes account of the indistinguishability of the particles. For an ideal gas, $V_N(\mathbf{r}^N) = 0$, the two particle density reduces to

$$\rho_N^{(2)}(\mathbf{r}_1, \mathbf{r}_2) = \rho^2 (1 - \frac{1}{N}). \tag{2.5}$$

The (dimensionless) pair distribution function $g_N^{(2)}(\mathbf{r}_1, \mathbf{r}_2)$ is defined in terms of the two-particle density as

$$g_N^{(2)}(\mathbf{r}_1, \mathbf{r}_2) = \frac{\rho_N^{(2)}(\mathbf{r}_1, \mathbf{r}_2)}{\rho_N^{(1)}(\mathbf{r}_1) \rho_N^{(1)}(\mathbf{r}_2)}. \tag{2.6}$$

If the system is both homogeneous and isotropic then $g_N^{(2)}(\mathbf{r}_1, \mathbf{r}_2)$ is a function only of the distance $r = |\mathbf{r}_1 - \mathbf{r}_2|$ - called the radial distribution function and simply written as $g(r)$. A more illustrative interpretation of the definition (2.6) is the following: given a reference particle at the origin then $g(r)$ is the factor by which the mean number of particles, $4\pi r^2 dr \rho g(r)$, in a spherical shell of radius r and thickness dr centered around the reference particle deviates from the ideal gas value, $4\pi r^2 dr \rho$, due to interactions between the particles. If the repulsion between two particles is large at small distances, $g \to 0$ as $r \to 0$. For distances r much larger than the range of the interaction potential, the particles become uncorrelated and the pair distribution function approaches the ideal gas limit (2.5)

$$g(r) \to 1 - \frac{1}{N} \quad \text{for} \quad r \to \infty, \tag{2.7}$$

or, in the thermodynamic limit $g(r) \to 1$. In a typical simple liquid $g(r)$ is for large distances an oscillating function around 1 and shows for short and intermediate distances a series of peaks (see fig. (2.1)) which correspond to first neighbors, second neighbor shells, etc. and express the short range order that exists in a liquid.

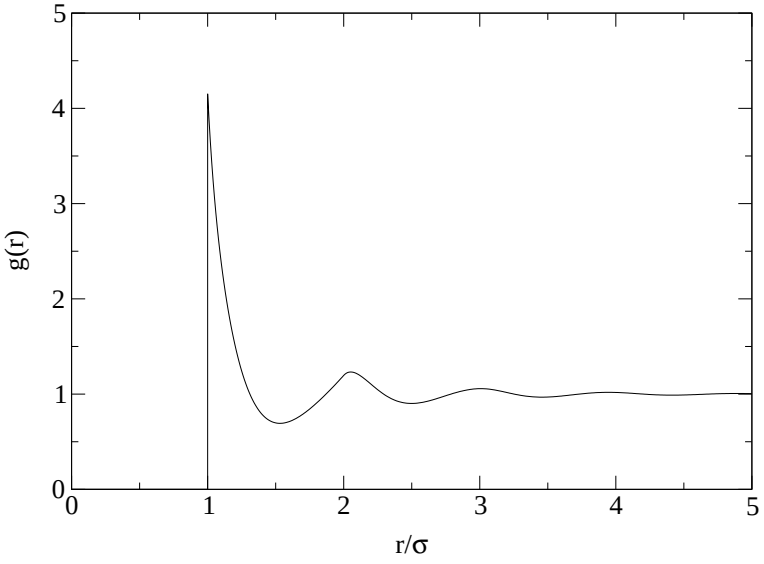

Figure 2.1: Typical pair distribution function of a hard-core system.

Let us assume in the following that the particles interact through central pair forces, thus

$$V_N(\mathbf{r}^N) = \sum_{i<j} \phi(r_{ij}), \quad r_{ij} = |\mathbf{r}_i - \mathbf{r}_j|, \quad i, j \in \{1 \ldots, N\}, \tag{2.8}$$

where $\phi(r)$ is the pair potential. Then thermodynamic properties can be expressed as integrals over $g(r)$ via three different routes [4].

One of them is the internal energy route according to which the excess (over ideal) part of the internal energy U^{ex} can be written as

$$\frac{U^{ex}}{N} = \frac{1}{N}\left\langle V_N(\mathbf{r}^N)\right\rangle = 2\pi\rho\int g(r)\phi(r)r^2dr. \tag{2.9}$$

In the second route the equation of state is obtained as an average over the virial

$$\begin{aligned}\frac{\beta P}{\rho} &= 1-\frac{\beta}{3N}\left\langle\sum_i \mathbf{r}_i\nabla_i V_N(\mathbf{r}^N)\right\rangle \\ &= 1-\frac{2}{3}\pi\beta\rho\int g(r)r^3\phi'(r)dr\end{aligned} \tag{2.10}$$

and therefore it is known as the virial route. The third possibility can be derived in the grand canonical ensemble and reads

$$1+\rho\int\left(g(r)-1\right)d^3r = \frac{1}{N}\left\langle(N-\langle N\rangle)^2\right\rangle = \rho k_B T\chi_T, \tag{2.11}$$

where

$$\chi_T = -\frac{1}{V}\left(\frac{\partial V}{\partial P}\right)_T = \left[\rho\left(\frac{\partial P}{\partial\rho}\right)_T\right]^{-1} \tag{2.12}$$

is the isothermal compressibility of the system. Eq. (2.11) is known as the compressibility equation.

Now three routes are available to determine the equation of state $\beta P/\rho$ starting from the pair distribution function. One of them leads to the pressure directly via the virial equation (2.10). We will use the notation P_V for the pressure obtained in this way. The second possibility is given via the compressibility equation (2.11). Integrating $\frac{1}{\rho\chi_T}$ with respect to the density along an isothermal path yields the pressure. In the following, we will denote the pressure obtained in this way by P_C. The third route is based on the excess internal energy U^{ex} as given by the energy route (4.24). U^{ex} is related to the excess (over ideal) Helmholtz free energy F^{ex} by the equation

$$U^{ex} = \left(\frac{\partial\beta F^{ex}}{\partial\beta}\right)_V. \tag{2.13}$$

Thus βF^{ex} can be obtained by integrating U^{ex} with respect to the inverse temperature along an isochore. By differentiating F^{ex} one obtains the excess (over ideal) pressure via

$$P^{ex} = -\left(\frac{\partial F^{ex}}{\partial V}\right)_T = \rho^2\left(\frac{\partial F^{ex}/N}{\partial\rho}\right)_T. \tag{2.14}$$

We will use the notation P_E for the pressure obtained via the energy route.

If the exact $g(r)$ were known from some liquid-state theory, then the value of the pressure obtained via the virial, the compressibility and the energy equation should be the same, i.e. $P_V = P_C = P_E$. The theory is then called thermodynamically self-consistent. However, integral equation or perturbation theories only yield, as a consequence of the approximations in their concepts, an approximate $g(r)$ and thus are, more or less, thermodynamically inconsistent. So the liquid-vapor coexistence curves obtained from the different routes will not coincide, with different values of the critical point parameters. E. g., the MSA is known to be highly inconsistent [11]: the curve of diverging compressibility falls well inside the liquid-vapor coexistence curve obtained from the energy route. Liquid-state theories that enforce thermodynamic consistency will be presented in chapter 4.1.

2.1.2 Total correlation function

We introduce the so called total correlation function $h(r)$ by subtracting from the pair distribution function its ideal gas value

$$h(r) = g(r) - 1. \tag{2.15}$$

Thus $h(r) \to 0$ for $r \to \infty$.

In order to describe the correlation between density fluctuations $\delta\rho(\mathbf{r}) = \rho(\mathbf{r}) - \langle\rho(\mathbf{r})\rangle$ at $\mathbf{r}$ and $\mathbf{r}'$ we introduce the density-density correlation function

$$\Gamma(\mathbf{r}, \mathbf{r}') = \langle\delta\rho(\mathbf{r})\delta\rho(\mathbf{r}')\rangle\,. \tag{2.16}$$

By inserting the local particle density (2.1) it follows that

$$\Gamma(\mathbf{r}, \mathbf{r}') = \rho_N^{(2)}(\mathbf{r}, \mathbf{r}') + \rho_N^{(1)}(\mathbf{r})\delta(\mathbf{r} - \mathbf{r}') - \rho_N^{(1)}(\mathbf{r})\rho_N^{(1)}(\mathbf{r}'); \tag{2.17}$$

in the homogeneous isotropic case we obtain $\Gamma(r) = \rho^2 h(r) + \rho\delta(r)$. The Fourier transform of $\Gamma(r)$ is known as the static structure factor

$$S(\mathbf{k}) = \frac{\widetilde{\Gamma}(\mathbf{k})}{\rho} = 1 + \rho\tilde{h}(\mathbf{k}), \tag{2.18}$$

where the Fourier transform is defined as

$$\tilde{h}(\mathbf{k}) = \int h(r)e^{-i\mathbf{kr}}d^3r. \tag{2.19}$$

The $k = 0$ limit of $S(\mathbf{k})$ is thus related to the isothermal compressibility (2.11)

$$S(0) = \rho k_B T \chi_T. \tag{2.20}$$

2.1.3 Ornstein-Zernike relation

The Ornstein Zernike (OZ) relation [12] defines the direct correlation function $c^{(2)}(\mathbf{r}_1, \mathbf{r}_2)$ in terms of the total correlation function $h^{(2)}(\mathbf{r}_1, \mathbf{r}_2)$

$$h^{(2)}(\mathbf{r}_1, \mathbf{r}_2) = c^{(2)}(\mathbf{r}_1, \mathbf{r}_2) + \int dr_3^3 \rho^{(1)}(\mathbf{r}_3) c^{(2)}(\mathbf{r}_1, \mathbf{r}_3) h^{(2)}(\mathbf{r}_3, \mathbf{r}_2). \tag{2.21}$$

The name direct correlation function for $c^{(2)}(\mathbf{r}_1, \mathbf{r}_2)$ can be motivated as follows: solving the OZ equation (2.21) iteratively, leads to

$$\begin{aligned} h^{(2)}(\mathbf{r}_1, \mathbf{r}_2) &= c^{(2)}(\mathbf{r}_1, \mathbf{r}_2) + \int dr_3^3 \rho^{(1)}(\mathbf{r}_3) c^{(2)}(\mathbf{r}_1, \mathbf{r}_3) c^{(2)}(\mathbf{r}_3, \mathbf{r}_2) \\ &\quad + \iint dr_3^3 dr_4^3 \rho^{(1)}(\mathbf{r}_3) \rho^{(1)}(\mathbf{r}_4) c^{(2)}(\mathbf{r}_1, \mathbf{r}_3) c^{(2)}(\mathbf{r}_3, \mathbf{r}_4) c^{(2)}(\mathbf{r}_4, \mathbf{r}_2) + \ldots \end{aligned} \tag{2.22}$$

Thus the total correlation between two particles is given by the direct correlation plus an indirect correlation mediated via an increasing number of intermediate particles.

For a homogeneous isotropic fluid the OZ relation takes the form

$$h(r) = c(r) + \rho \int dr'^3 c(r') h(|\mathbf{r} - \mathbf{r}'|), \tag{2.23}$$

which has a simpler form in Fourier space

$$1 + \rho \tilde{h}(k) = \left(1 - \rho \tilde{c}(k)\right)^{-1}. \tag{2.24}$$

So from the compressibility equation (2.11) it follows that

$$\rho \tilde{c}(0) = 1 - \frac{1}{\rho k_B T \chi_T}. \tag{2.25}$$

Thus $\tilde{c}(0)$ is finite and hence $c(r)$ is a short ranged function even at the critical point where the correlation length of density fluctuations and the isothermal compressibility diverges.

2.1.4 Extension to mixtures

The definitions and relations presented in the previous subsection for a one-component fluid can be generalized in a straightforward way to multi-component fluids. Since we will also be concerned with the thermodynamics and the phase behavior of binary mixtures we will briefly summarize these basic relations.

We consider a homogeneous isotropic fluid consisting of m components and particle numbers N_i, $i = 1, \ldots, m$. $\rho_i = \frac{N_i}{N}$ denotes the partial number density of the i^{th} species,

$\rho = \sum_i \rho_i$ the total number density and $x_i = \frac{\rho_i}{\rho}$ is the mole fraction (or number concentration) of the i^{th} component in the mixture. Thus $\sum_i x_i = 1$ The structure of the fluid is described by the set of $\frac{1}{2}m(m-1)$ radial distribution functions $\{g_{ij}(r)\}$, which satisfy the symmetry relations $g_{ij}(r) = g_{ji}(r)$. These functions have the following meaning: given a particle of species i at the origin then $4\pi r^2 dr g_{ij}(r)\rho_j$ is the mean number of particles of species j found in a distance r apart. The radial distribution functions satisfy the symmetry relations $g_{ij}(r) = g_{ji}(r)$. Similarly to eq. (2.18) one can define the partial structure factors as

$$S_{ij}(k) = \sqrt{x_i x_j}\delta_{ij} + x_i x_j \rho \tilde{h}_{ij}(k), \tag{2.26}$$

where $h_{ij}(r) = g_{ij}(r) - 1$. The multicomponent OZ equations read

$$h_{ij}(r) = c_{ij}(r) + \sum_{k=1}^{m} \rho_k \int d^3r' c_{ik}(|\mathbf{r} - \mathbf{r}'|)h_{kj}(r'), \tag{2.27}$$

where the $c_{ij}(r)$ are the direct correlation functions between particles of species i and j. Hence,

$$\sqrt{x_i x_j}\delta_{ij} - \rho x_i x_j \tilde{c}_{ij}(k) = \left(\mathsf{S}^{-1}\right)_{ij}, \tag{2.28}$$

where the matrix notation $\mathsf{S} = (S_{ij})$ was introduced.

The generalization to mixtures of the internal energy route reads

$$\frac{U^{ex}}{V} = 2\pi \sum_i \sum_j \rho_i \rho_j \int g_{ij}(r)\phi_{ij}(r) r^2 dr \tag{2.29}$$

and of the compressibility route

$$\frac{1}{\rho k_B T \chi_T} = 1 - \frac{1}{\rho} \sum_{ij} \rho_i \rho_j \tilde{c}_{ij}(0). \tag{2.30}$$

Equivalent results for the partial direct correlation functions are

$$-\sqrt{\rho_i \rho_j} \left(\frac{\partial \beta \mu_i}{\partial \rho_j}\right)_{V,T,\rho_{i\neq j}} = \delta_{ij} - \rho \tilde{c}_{ij}(0), \tag{2.31}$$

where μ_i is the chemical potential of species i.

Appropriate linear combinations of the structure factors S_{ij} that correspond to the correlations between fluctuations in the density and concentration have been introduced in [13] and will be presented in the following. We will restrict the considerations to the simpler binary mixture where the number concentrations of the two components are $x_1 \equiv x$ and $x_2 = 1 - x$.

We define the fluctuations of the total density as

$$\delta\rho(\mathbf{r}) = \delta\rho_1(\mathbf{r}) + \delta\rho_2(\mathbf{r}), \tag{2.32}$$

where $\delta\rho_i(\mathbf{r}) = \rho_i(\mathbf{r}) - \rho_i$ is the fluctuation of the local density of particle species i around its average value ρ_i. Similarly, we define the concentration fluctuation

$$\delta c(\mathbf{r}) = \frac{x_2\delta\rho_1(\mathbf{r}) - x_1\delta\rho_2(\mathbf{r})}{\rho}. \tag{2.33}$$

Then the following structure factors express the correlations between total density fluctuations, concentration fluctuations and the cross correlations between density and concentration fluctuations:

$$\begin{aligned}
S_{NN}(k) &= \frac{1}{\rho}\mathcal{FT}\left[\langle\delta\rho\cdot\delta\rho\rangle\left(|\mathbf{r}-\mathbf{r}'|\right)\right] = S_{11}(k) + S_{22}(k) + 2S_{12}(k) \\
S_{CC}(k) &= \rho\mathcal{FT}\left[\langle\delta c\cdot\delta c\rangle\left(|\mathbf{r}-\mathbf{r}'|\right)\right] = x_2^2 S_{11}(k) + x_1^2 S_{22}(k) - 2x_1x_2S_{12}(k) \\
S_{NC}(k) &= \mathcal{FT}\left[\langle\delta c\cdot\delta\rho\rangle\left(|\mathbf{r}-\mathbf{r}'|\right)\right] = x_2 S_{11}(k) - x_1 S_{22}(k) + (x_2 - x_1)S_{12}(k),
\end{aligned} \tag{2.34}$$

where $\mathcal{FT}[\cdot]$ denotes the Fourier transform of the expression in the brackets. The generalization of eq. (2.20) to the binary mixture case are the following relationships between the long-wavelength limits of the structure factors defined in (2.34) and thermodynamic properties [13]

$$S_{CC}(0) = NkT/\left(\frac{\partial^2 G}{\partial x^2}\right)_{T,P,\rho} \tag{2.35}$$

$$S_{NN}(0) = \rho k_B T\chi_T + \delta^2 S_{CC}(0) \tag{2.36}$$

$$S_{NC}(0) = -\delta S_{CC}(0), \tag{2.37}$$

where G is the Gibbs free energy, and $\delta = \rho(v_1 - v_2)$. $v_i = \left(\frac{\partial V}{\partial N_i}\right)_{P,T,N_{j\neq i}}$ is the partial molar volume of species i.

2.2 Liquid-State Techniques

We have shown in the preceeding subsection that the pair distribution function $g(r)$ plays a central role in liquid-state theories since once this function is known thermodynamic quantities can be calculated. In order to determine $g(r)$ for a system with a given interatomic pair potential some approximation must be made. In this section we will present those liquid-state approximations that are relevant for our work, the MSA and the LOGA/ORPA. They represent examples of two different approximate schemes,

namely integral equation theories (IETs) and perturbation theories (PTs). In the following we will briefly introduce the basic ideas of these two groups of liquid-state theories, a more detailed description (including the derivation of those relations) can, f. i., be found in [4].

2.2.1 Integral Equation Theories

From a cluster expansion of $g(r)$ [4] it follows that

$$g(r) = e^{-\beta\phi(r)+h(r)-c(r)+E(r)}, \tag{2.38}$$

introducing the so-called brigde function $E(r)$. Eq. (2.38) can be considered as an exact closure relation to the OZ equation if the exact $E(r)$ were known. Then we have a set of two equations in the two unknowns $c(r)$ and $h(r)$ for a given pair potential $\phi(r)$. An approximate closure relation is obtained by introducing either an approximation for $E(r)$ or, instead of assuming an approximation for $E(r)$, one could also derive an approximate closure relation to the OZ equation from exact relations of statistical mechanics, introducing simplifying assumptions; this leads to a functional relation between $h(r)$ and $c(r)$, including the pair potential $\phi(r)$, i.e.

$$F(c(r), h(r), \phi(r)) = 0. \tag{2.39}$$

So $h(r)$ and $c(r)$ are then determined by solving the OZ integral equation (2.23) supplemented by some closure relation (2.39).

Various closure relations have been derived by using diagrammatic expansions or functional Taylor expansions [4], like e.g. the well known Percus-Yevick (PY) closure relation which assumes that

$$c(r) = \left(1 - e^{\beta\phi(r)}\right) g(r). \tag{2.40}$$

For a hard-sphere (HS) fluid with interaction potential

$$\phi(r) = \begin{cases} \infty & r < \sigma \\ 0 & r > \sigma \end{cases}, \tag{2.41}$$

where σ is the HS diameter it follows from (2.40), (2.41) and (2.38) that

$$\begin{aligned} c(r) &= 0 \quad r > \sigma \\ g(r) &= 0 \quad r < \sigma. \end{aligned} \tag{2.42}$$

The second relation, the so called core condition is exact and expresses the fact that the HSs are not allowed to overlap. The OZ equation (2.23) with the closure relation (2.42) is analytically solvable (see e.g. [4]).

Another approximation, that is very frequently used due to its semi-analytic solubility for pair potentials like the HS Yukawa potential [14], charged HSs [15], dipolar HSs [16], sticky HSs [17] and a generalized HS Yukawa potential [18] is the mean spherical approximation (MSA). The conventional MSA is only applicable to systems where the pair potential consists of a hard-core (HC). So, let us assume in the following a HC potential with HC diameter σ and some tail

$$\phi(r) = \begin{cases} \infty & r < \sigma \\ w(r) & r > \sigma \end{cases} . \tag{2.43}$$

From cluster expansion [4] it follows that the asymptotic behavior of the direct correlation function is given by

$$c(r) \to -\beta\phi(r) \quad \text{for} \quad r \to \infty. \tag{2.44}$$

Thus $c(r)$ behaves at long range as the interparticle potential. The approximation in the MSA scheme is the assumption that the relation (2.44) is valid also for short distances. So the MSA reads

$$\begin{aligned} c(r) &= -\beta w(r) \quad r > \sigma \\ g(r) &= 0 \quad r < \sigma. \end{aligned} \tag{2.45}$$

In the case of a pure HS interaction the MSA reduces to the PY approximation.

2.2.2 Perturbation Theories, LOGA/ORPA

The basic idea of PTs is a separation of the pair potential into a harsh, short-ranged repulsion and a smoothly varying long-ranged attraction. It is known that the repulsive part mainly determines the structure of a fluid while the attractive part plays a minor role and can therefore be treated as a perturbation of the repulsive reference system leading to (small) corrections of the thermodynamic and structural properties [19]. Furthermore, it is rather convenient to approximate the repulsion by the infinitely steep repulsion of the HS potential, since the HS fluid represents a reference system whose structural and thermodynamic properties are known with great accuracy.

Thus in the spirit of a perturbation theory one can regard - in the simplest approximation - a fluid as a system of HSs that move in a uniform attractive background. In this approximation one arrives at the famous van der Waals equation. Higher order approximations can be obtained by expanding the Helmholtz free energy either in powers of the strength of the perturbation (λ-expansion) or in powers of the interaction range (γ-expansion) [4].

The perturbation theory which is used in the present work, the LOGA/ORPA [20, 21, 22], is applicable to fluids (and their mixtures) where the interactions between particles are pairwise additive. It assumes that the pair potential ϕ between particles is split up into

$$\phi(r) = \phi_r(r) + \phi_p(r), \tag{2.46}$$

where $\phi_r(r)$ is the pair potential of the reference system and $\phi_p(r)$ is the attractive perturbation. Since in the present work we consider exclusively HC interactions it is most obvious that the $\phi_r(r)$ are represented by HS potentials characterized by the HS diameter σ. This defines the $\phi_p(r)$ apart from finite variations inside the core. In the case where $\phi_r(r)$ is not a HS potential, the softness of the potential can be taken into account via the Weeks-Chandler-Andersen 'blip'-function expansion [23].

The separation of the potential leads naturally to the decomposition of all the correlation functions

$$h(r) = h_r(r) + h_p(r) \tag{2.47}$$

and

$$c(r) = c_r(r) + c_p(r), \tag{2.48}$$

where $h_r(r)$ and $c_r(r)$ are the correlation functions of the reference fluid and $h_p(r)$ and $c_p(r)$ are the corrections to the correlation functions of the reference system due to the attractive interaction.

In the random phase approximation (RPA) one assumes that

$$c_p(r) = -\beta\phi_p(r). \tag{2.49}$$

However, this approximation does not guarantee that $g(r)$ vanishes inside the HC as it should in an exact theory. This means that geometrical exclusion effects are not treated correctly. On the other hand, in this framework, there is a flexibility in the choice of $\phi_p(r)$ that can usefully be exploited: It is clear that eq. (2.46) does not define the perturbation uniquely for $r < \sigma$. For this physically inaccessible region, the perturbation can be chosen to have any finite functional form. Thus the perturbing potential $\phi_p(r)$ inside the hard

core ($r < \sigma$) can be varied to obtain the so called optimized potential. We thus obtain the LOGA/ORPA which is formulated via the two relations:

$$c_p(r) = -\beta\phi_p(r) \quad \text{for} \quad r > \sigma \tag{2.50}$$

and the perturbation potential inside the core is chosen so that

$$g_p(r) = h_p(r) = 0 \quad \text{for} \quad r < \sigma. \tag{2.51}$$

The LOGA/ORPA is therefore similar to the MSA, the only difference is the exact treatment of the hard-sphere reference system in the LOGA/ORPA.

Chapter 3

Phase Coexistence

3.1 Phase Behavior and Stability Conditions

3.1.1 One-component System

A typical phase diagram of a one-component substance in the P-T and T-ρ plane is shown in fig. (3.1). The liquid phase exists only in the small part of the entire P-ρ-T space that is bounded above by a critical point where coexisting vapor and liquid become identical and below by a triple point. Above the critical point there exists only a single fluid phase and there is a continuous path from the gas via the fluid to the liquid phase as indicated in the figure. This is not the case for the transition from liquid to solid that does not end at a critical point. Consider moving along the gas-liquid coexistence line in the direction of increasing temperature, then the difference in density between the gas and the liquid decreases continously to zero and becomes zero at the critical point. The density difference $\Delta\rho = \rho_l - \rho_v$ between the coexisting liquid and gas phase, which is nonzero below the critical temperature, is called the order parameter of the gas-liquid coexistence transition.

In general, the conditions for coexistence of two phases in contact with each other [24, 25] are

$$T = T', \quad P = P', \quad \mu = \mu', \tag{3.1}$$

where the primed and unprimed quantities T, P, μ are the temperature, pressure and chemical potential of the two phases. The first condition expresses thermal equilibrium, the second mechanical equilibrium and the third material equilibrium between two phases. From the Gibbs rule it follows that a one-component system cannot have more than three

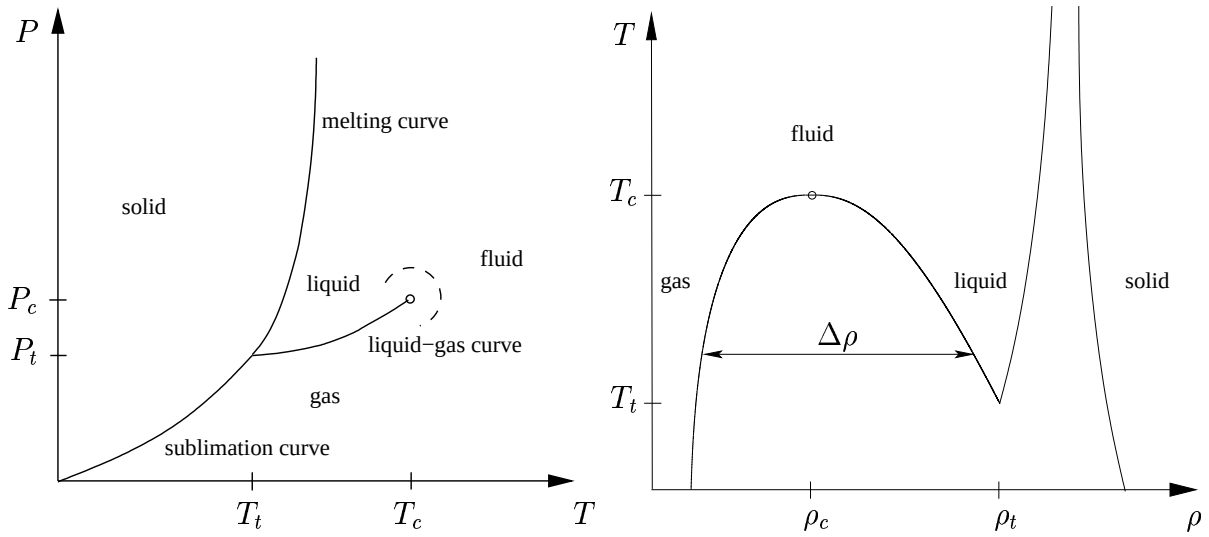

Figure 3.1: Left: Phase diagram of a one-component system in the P-T plane. The indices 't' and 'c' indicate the triple and critical point. The gas-liquid coexistence curve ends at a critical point. So there is a continuous path from the gas to the liquid phase as indicated by the dashed line. Right: Gas-liquid coexistence curve for a one-component substance in the T-ρ plane. The indices 't' and 'c' indicate the triple and critical point. The order parameter of the gas-liquid transition, $\Delta\rho = \rho_l - \rho_v$, vanishes at the critical point.

coexisting phases and that the coexistence of three phases can only appear at a single point, the triple point.

The coexistence curves in the $T-\rho$ plane can be determined by expressing the chemical potential and the pressure as functions of the density at fixed temperature T and solving the coupled set of equations

$$\mu(\rho, T) = \mu(\rho', T) \tag{3.2}$$

$$P(\rho, T) = P(\rho', T) \tag{3.3}$$

for ρ and ρ'. This route was chosen in the present work. Equivalent routes are the well-known Maxwell construction see fig. (3.2) and the common tangent construction for the Helmholtz free energy per volume F/V as a function of the density.

The condition of phase stability for a one-component system is

$$\left(\frac{\partial^2 F}{\partial V^2}\right)_{T,N} = -\left(\frac{\partial P}{\partial V}\right)_{T,N} = \frac{1}{V\chi_T} > 0, \tag{3.4}$$

meaning that the pressure cannot decrease with increasing density. The points where χ_T diverges define the so-called spinodal line that separates the stable from the unstable

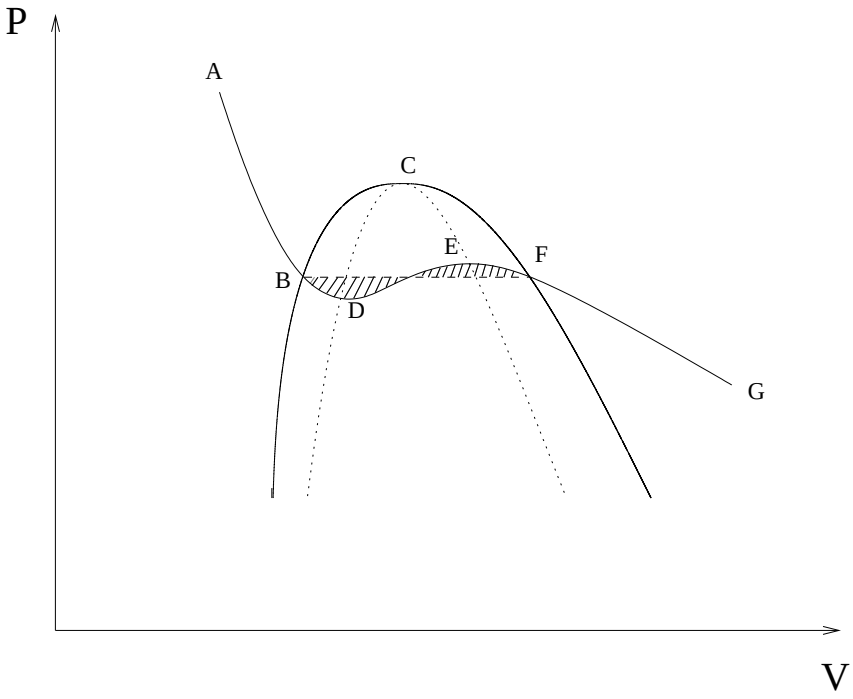

Figure 3.2: Van der Waals construction to determine phase equilibria along an isotherm (ABDEFG). The shaded areas enclosed by the curve linking BDEF and the dashed line are equal and indicate the Maxwell construction. B and F are points of the liquid-vapor coexistence curve (binodal) - full line, D and E points of the spinodal line, where $\chi_T = \infty$ corresponding to a local maximum and minimum of the isotherms - dotted line. The binodal and spinodal curve touch each other at the critical point C. Along the curves BD and EF the system is metastable ($\chi_T > 0$), while it is mechanically unstable along the curve DE ($\chi_T < 0$).

region. In the stable region, where $\chi_T > 0$, the system can exist in a single phase while inside the other region the free energy can be lowered by phase separation into two phases with different density. Thus the single phase gets unstable and phase separation occurs.

3.1.2 Binary Mixtures

The phase behavior of binary mixtures is of course much richer than that of a simple one-component substance. Depending on the relative sizes of the two particle species and the strength of their interactions one observes a large variety of different phase diagrams [5]. A systematic study of the different phase diagram topologies was performed by Konynenburg and Scott by using the van der Waals equation of state [26]. Even for the simple case of

equally sized particles they identified not less than 12 different types of phase diagrams distinguished by the presence and absence of three-phase lines and azeotrope lines, by the number of critical lines and by the way the critical lines terminate.

The conditions for phase equilibrium generalize to the case of a two-component system with concentrations $x_1 \equiv x$ and $x_2 = 1 - x$ by requiring that

$$T = T', \quad P = P', \quad \mu_1 = \mu_1', \quad \mu_2 = \mu_2'. \tag{3.5}$$

At an azeotropic point two phases with the same composition are in equilibrium, hence additionally to the usual coexistence conditions the condition $x = x'$ must be fulfilled. According to the Gibbs rule up to four phases can coexist in a binary mixture; four phases coexist in a point and three phases can coexist along a line (triple line).

The conditions of phase coexistence and phase stability are expressible in terms of the Gibbs free energy G. Similarly to the common tangent construction for the Helmholtz free energy F in the one-component case, the concentrations x and x' of two coexisting phases at a given temperature T and pressure P can be obtained via a common tangent construction of the Gibbs free energy as a function of x. The concentration of two coexisting phases at fixed pressure P can be reported in a $T - x$ diagram. Various types of diagrams are distinguishable depending on the number and loci of the critical points [5].

For a given composition, density and temperature, a fluid mixture can be present in a single homogeneous phase only if thermodynamic stability is satisfied. In contrast to a one-component system where only mechanical stability, expressed via $\chi_T > 0$, must be satisfied, a fluid mixture must have both mechanical (or liquid-vapor) stability and material (or liquid-liquid) stability. The latter is expressed via

$$\left(\frac{\partial^2 G}{\partial x^2}\right)_{T,P,\rho} \geq 0. \tag{3.6}$$

If this condition is not satisfied then the Gibbs free energy can be decreased - while keeping temperature and pressure constant - by phase separation into two phases of different compositions: this phase separation is called demixing transition.

While the first kind of instability where χ_T diverges and which forces the fluid to phase separate into two phases of different densities is associated with a divergence of $S_{NN}(0)$ (see (2.36)), the material instability corresponds to a divergence of the correlation length of concentration fluctuations and thus $S_{CC}(0)$ (see eq. (2.35)). The spinodal line of a mixture is thus located at those points where either $S_{CC}(0)$ or $S_{NN}(0)$ or both diverge. In the case in which a mixture is mechanically unstable, but materially stable,

i.e. at an azeotropic instability, $S_{CC}(0)$ remains finite and $S_{NN}(0)$ diverges leading to a separation into two phases of different densities but equal compositions. So it follows from (2.26) and (2.34) that at an azeotropic instability $\tilde{h}_{12}(0) = \frac{1}{2}\left(\tilde{h}_{11}(0) + \tilde{h}_{22}(0)\right)$ and $S_{CC}(0) = x_1 x_2$. Furthermore, from eq. (2.37) it follows that $v_1 - v_2 = \frac{1}{2}\left(\tilde{h}_{11}(0) - \tilde{h}_{22}(0)\right)$. From eqs. (2.35– 2.37) one sees that a divergence of $S_{CC}(0)$ also causes a divergence of the other structure factors, so it is not straightforward to distinguish in the general case of a binary mixture the two kinds of instability. The situation is different in the case of a so-called binary symmetric mixture (see section 4.5.2).

In the following we will restrict our investigations to this simpler model system.

3.1.3 Binary Symmetric Fluid

In the binary symmetric mixture the like-particle interactions are identical ($\phi_{11}(r) = \phi_{22}(r) \quad \forall r$), while the unlike interactions are different from the like ones ($\phi_{12}(r) \neq \phi_{ii}(r), i = 1, 2$). We further assume that the functional form of the like and unlike interactions is equal. Only the strength is different, i.e.,

$$\phi_{11}(r) = \phi_{22}(r) \tag{3.7}$$

$$\phi_{12}(r) = \alpha\phi_{11}(r), \tag{3.8}$$

where α is the relative strength of interactions between particles of dissimilar and similar species.

Due to the symmetry of the potentials one obtains symmetry relations for the structural and thermodynamic properties, like for instance

$$h_{11}(r; T, \rho, x) = h_{22}(r; T, \rho, 1 - x)$$

$$h_{12}(r; T, \rho, x) = h_{12}(r; T, \rho, 1 - x)$$

$$\mu_1(T, \rho, x) = \mu_2(T, \rho, 1 - x) \tag{3.9}$$

$$P(T, \rho, x) = P(T, \rho, 1 - x) \quad \text{etc.} \tag{3.10}$$

Although such a model system seems rather artifical and does not allow the description of an experimentally observed phase behavior [1] it shows already a rather rich variety of phase behavior and offers insight into the link between the microscopic description of a system and its phase behavior. The advantage of this simple model is the fact that its

[1] An example for a realistic system with such a symmetry are mixtures of d,l-optical isomers. However, liquid-liquid separations in these systems have not been reported so far (see page 524 of [26]).

interactions are characterized by only a few parameters, namely the interaction strength ratio α and the parameters of the pair potential ϕ_{11}: they trigger the phase behavior of the system, so that a systematic investigation of their influence is still within reach. On the other hand - despite the simplicity of the model - the phase diagrams show nevertheless a much richer variety than those of a one-component system and interesting phenomena, like the existence of triple points, critical lines, critical end points and tricritical points.

From the different possibilities to present phase diagrams, we have chosen in this work presentations in the $T-\rho-x$ space, their projections onto the $T-\rho$ plane and their isothermal slices leading to phase diagrams in the $\rho-x$ plane.

In the work we restrict ourselves to the determination of those coexisting phases where the number of species 1 and species 2 particles is equal, i.e. we consider only those phase equilibria where $x' = 1 - x$. In that case four different types of phase diagrams can be observed that belong to two classes.

1. The first class, where the similar species interaction is favorable, i.e. $\alpha < 1$, is characterized by the presence of a critical line of demixing transitions (the so called λ-line). For a given density there is a critical point of the demixing transition (critical consolute point) at some finite temperature T_c. The symmetry of our system implies that this critical point is located at $x = 1/2$. Above this temperature one observes a homogeneous mixture of 1 and 2 particles ($x = x' = 1/2$) - the so called mixed fluid (MF) - while below T_c the liquid separates into a 1-rich phase with concentration x and a 2-rich phase whose concentration is $x' = 1 - x$ - the so called demixed fluid (DF).

2. The second class, where $\alpha \geq 1$, is characterized by the absence of a critical line and the absence of demixing transitions.

A system of the first class exhibits in addition to these demixing transitions also liquid-vapor transitions as a one-component fluid. Depending on the interplay of these two types of phase transitions one can distinguish three types of phase diagrams that will be presented in the following. One of them is shown in fig. (3.3).

In the following we will use a simpler two-dimensional representation of the phase diagram which is obtained by the projection of the two high-density branches of the three-phase line along the x direction onto the $x = 1/2$ plane and omitting the demixing curves. Only the critical line of the demixing transitions (λ-line) will be shown. Owing to the symmetry of the system, the coexisting phases of the two high density branches of

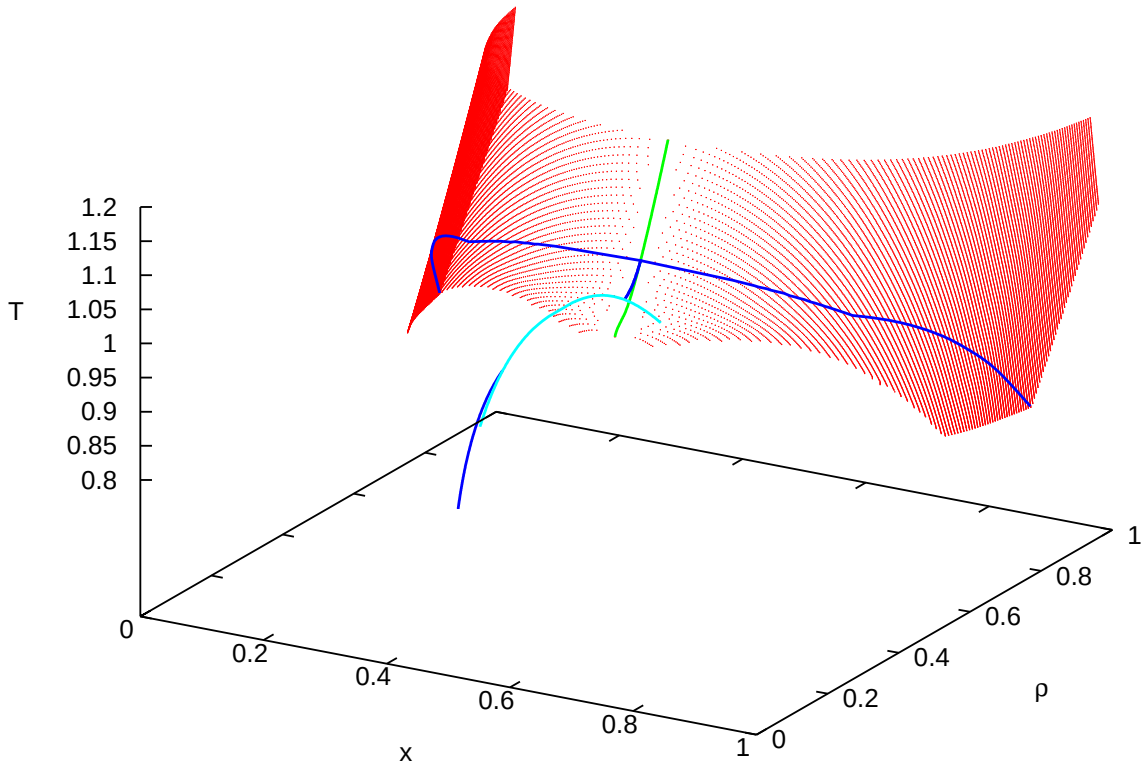

Figure 3.3: Phase diagram of type II (see text) of a binary symmetric fluid in the $T-\rho-x$ space. The phase diagram is symmetric with respect to the $x = 1/2$-plane. Red curves: demixing transitions. Green curve: λ-line. Light blue curve: VMF transition. Dark blue curve: VDF/MFDF transitions.

the three phase line have the same density and thus their projections yield only one line. Using this representation, fig. (3.4) shows a schematic drawing of the three different types of phase diagrams of class 1. The three types differ in the way the second order transition associated with demixing merges into the first order liquid-vapor (LV) transition:

Type I: Fig. (3.4a) shows the situation when the λ-line approaches the LV coexistence curve well below the critical point. In that case the λ-line intersects the first order LV curve at a critical end point (CEP). At the CEP, a critical liquid coexists with a noncritical vapor. Above the CEP temperature a vapor and a homogeneous liquid of intermediate density coexist becoming identical at the LV critical point. At higher

densities, as one crosses the λ-line, the fluid demixes. The full line below the CEP temperature is a triple line where a gas, a 1-rich and a 2-rich liquid coexist.

Type III: In fig. (3.4c) the λ-line intersects the LV line at the LV critical point. In that case the first order transition between the vapor and the mixed liquid is absent and the λ-line ends at a tricritical point where three phases become critical at the same time: a vapor, a 1-rich liquid and a 2-rich liquid. So two order parameters, namely $\Delta\rho = \rho_l - \rho_v$, where ρ_l and ρ_v are the coexisting liquid and vapor densities, and $\Delta x = x - x' = 2x - 1$ vanish at the same time. The tricriticality is a specific feature of the symmetric model. In a general binary fluid tricriticality does not occur (see [26]).

Type II: The intermediate situation is shown in fig. (3.4b) where the λ-line approaches the LV coexistence curve slightly below the LV critical point. As in type I one finds a LV critical point and as in type III a tricritical point. Additionally this type is characterized by a triple point where – to be correct - four phases coexist: a vapor, a mixed liquid at intermediate density, a 1-rich and a 2-rich liquid at higher density.

In a mean field study [9] it was shown that the transition between the different types of phase diagrams is triggered by the parameter α.

Another type of phase diagram has been observed in grand canonical Monte Carlo (GCMC) simulations of a binary symmetric fluid inside a porous matrix [27], in which the λ-line intersects the LV critical line at a CEP on the vapor side (see fig. (3.5)). So above the CEP temperature one finds a four-phase line, where 1- and 2-rich phases of lower density coexist with 1- and 2-rich phases of higher densities. In the simulations the constraint of equal particle numbers was replaced by imposing equal chemical potentials for both species. So the demixed fluid phase that is observed comprises either a homogeneous 1-rich or 2-rich phase, which are - due to the symmetry - indistinguishable. Thus if the coexisting 1- and 2-rich phases are regarded as a single liquid phase (the demixed fluid) the 'four-phase' line would not violate the Gibbs rule.

Similar archetypes of phase diagrams (and sequences of these) are encountered in systems with completely different interatomic potentials: as examples we list here the *Heisenberg* fluid [28] (a fluid where the particles interact via hard-core and a *Heisenberg*-type interaction of their dipolar moments) and the *Stockmayer* fluid [29] (a fluid where the particles carry dipolar moments and interact - in addition - via Lennard-Jones potentials).

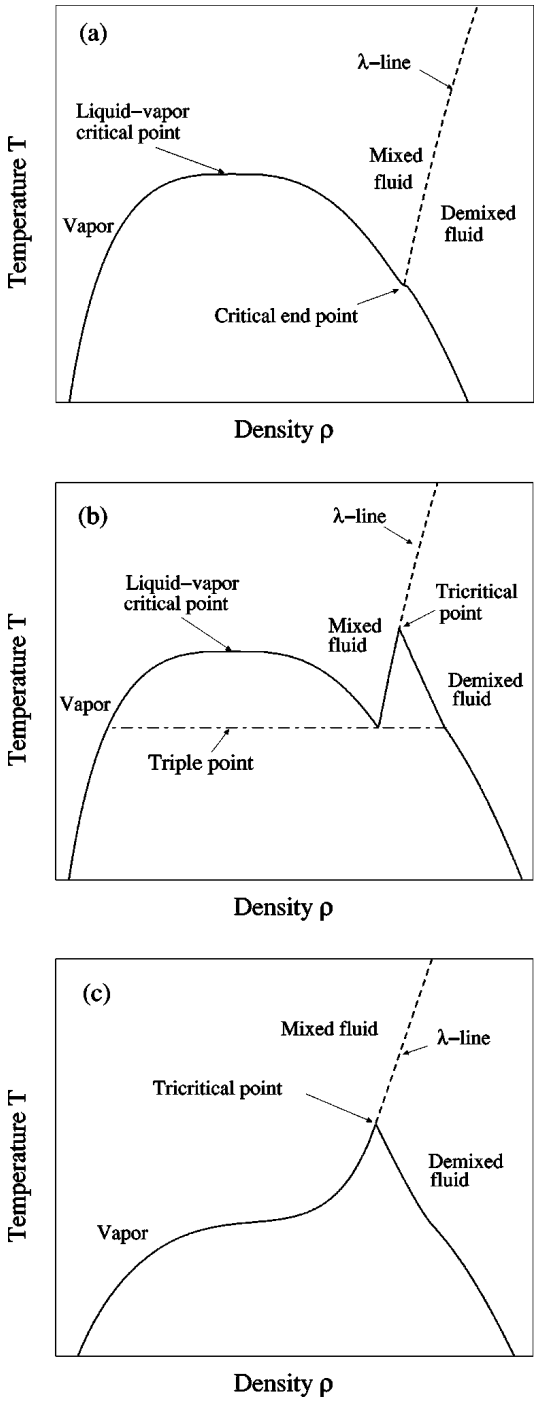

Figure 3.4: Schematic representation of the three types of phase diagrams of class 1 introduced in the text (from [9]). The phase diagrams are projections of the three-dimensional $T - \rho - x$ phase diagrams onto the $x = 1/2$-plane. The full curve is the liquid-vapor boundary. The dashed curve is the λ-line.

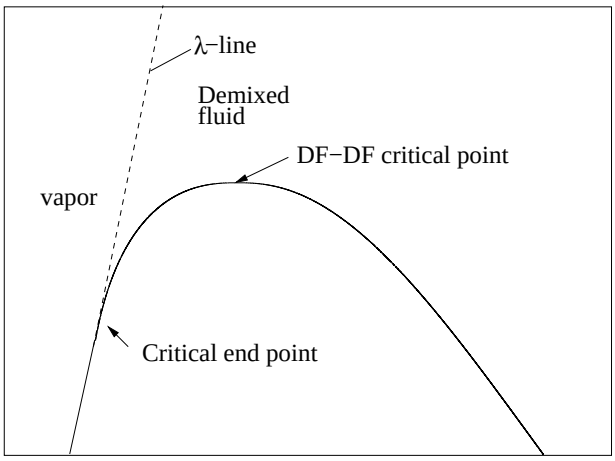

Figure 3.5: Schematic representation of the fourth type of phase diagram of class 1, that was observed in the GCMC studies of a binary symmetric fluid inside a porous matrix [27]. The full curve is the liquid-vapor boundary. The dashed curve is the λ-line.

Both, in the case of a binary mixture in the bulk and confined in a disordered porous matrix we have calculated the phase diagrams by equating, at a given temperature T, the pressure, P, and the chemical potentials, μ_i, of the coexisting phases. The general equilibrium conditions read

$$\mu_i(\rho, x, T) = \mu_i(\rho', x', T) \qquad i = 1, 2 \tag{3.11}$$

$$P(\rho, x, T) = P(\rho', x', T), \tag{3.12}$$

where the thermodynamic states of the coexisting phases are given by (ρ, x) and (ρ', x'). In the following we use the symmetry relations expressed in eqs. (3.9) and (3.10).

First the azeotrope line [2] is obtained by solving the set of equations

$$\mu_i(\rho, x = 1/2, T) \equiv \mu(\rho, x = 1/2, T) = \mu(\rho', x = 1/2, T)$$
$$P(\rho, x = 1/2, T) = P(\rho', x = 1/2, T). \tag{3.13}$$

For the V-MF and the MF-DF transitions we proceed in two steps. First we determine the phase diagram of the demixing transition, i.e. we search for two coexisting states with concentrations x and $x' = 1 - x$. Due to the symmetry eq. (3.10) $\rho' = \rho$ and due to eq. (3.9) equations (3.11) reduce to solving at a given temperature T and density ρ the equation

$$\mu_1(\rho, x, T) = \mu_2(\rho, x, T), \tag{3.14}$$

[2] It follows from the van der Waals study of [26] (see eq. (21) of this reference) that an azeotropic behavior in a binary symmetric mixture can only appear at $x = \frac{1}{2}$.

which defines the line $x(\rho)$ of the second order demixing transition - if it exists. Along this line the chemical potentials of the two species are equal by construction and denoted by $\mu(\rho, x(\rho), T)$. In a second step the solution of the two equations,

$$\mu(\rho, x = 1/2, T) = \mu(\rho', x(\rho'), T) \tag{3.15}$$

$$P(\rho, x = 1/2, T) = P(\rho', x(\rho'), T) \tag{3.16}$$

gives the density of the V or MF, ρ, and that of the DF, ρ', with concentrations $x(\rho')$ and $1 - x(\rho')$, in equilibrium.

Chapter 4

Self Consistent Liquid-State Methods

4.1 Introduction

As was pointed out already in Chapter 2.1.1 integral equation and perturbation theories suffer from a lack of thermodynamic consistency: that is, different routes to thermodynamics yield different results. Thus several integral equation theories have been modified in such a way that consistency between different routes is enforced.

One of these approaches is the generalized mean spherical approximation (GMSA) which is an extension of the MSA. It was introduced by Waisman [30] to improve the PY solution of hard spheres. He modified the PY ansatz $c(r) = 0$ for $r > \sigma$, by assuming a form of a Yukawa tail for $c(r)$ outside the HC, i.e.

$$c(r) = \frac{K}{r} e^{-z(r-\sigma)} \quad \text{for} \quad r > \sigma. \tag{4.1}$$

Waisman derived an analytic solution of the OZ equation supplemented by the exact core condition and the closure relation (4.1). Based on this analytic solution he chose the parameters K and z in order to fit the thermodynamics of this model to computer simulation data, parameterized in terms of the Carnahan Starling (CS) equation of state [31]. The radial distribution function so obtained considerably improved the PY one. Waisman's analytic solution was extended by Høye and Stell [32] to the case when the direct correlation function is a linear combination of two Yukawa tails.

$$c(r) = \frac{A_1}{r} e^{-z_1(r-\sigma)} + \frac{A_2}{r} e^{-z_2(r-\sigma)} \quad \text{for} \quad r > \sigma. \tag{4.2}$$

If one interprets the first Yukawa term as corresponding to the MSA closure relation for $c(r)$ outside the core for a system with the pair potential $\beta\phi(r) = -\frac{A_1}{r}e^{-z_1(r-\sigma)}$ then the second term can be viewed as a correction term as in the Waisman parameterization of $c(r)$ for hard spheres. Again there are two parameters A_2 and z_2 available either to fit thermodynamically consistent quantities, as given by computer simulation, or to satisfy the thermodynamic self-consistency relation without any further thermodynamic input. So this is a possibility to improve the MSA whose main deficiency is the substantial lack of thermodynamic consistency while retaining its great advantage of analytic solubility for hard-core Yukawa (HCY) systems.

A similar GMSA scheme was developed by Stell *et al.* for ionic and dipolar fluids [33]: There it was called a self-consistent Ornstein Zernike approximation (SCOZA) since self-consistency among the three thermodynamic routes (i.e. virial, energy and compressibility route) was enforced. However, in contrast to the SCOZA in its present version that we will introduce below, thermodynamic consistency was achieved by fitting the available GMSA parameters to some external set of data either given by a prescribed equation of state or obtained from computer simulations. In contrast, in the SCOZA with which we will be concerned below no supplementary thermodynamic or other input is necessary. Thus this scheme is entirely self-contained.

The thermodynamic consistency relations can be expressed in the form

$$\frac{\beta P_V}{\rho} = \frac{\beta P_C}{\rho} \tag{4.3}$$

$$\frac{\beta P_V}{\rho} = \frac{\beta P_E}{\rho}. \tag{4.4}$$

However, in most applications of liquid-state theories the first consistency relation is rather expressed as

$$\left(\frac{\beta\partial P_V}{\partial\rho}\right)_T = \frac{1}{\rho k_B T \chi_T}, \tag{4.5}$$

where χ_T is the isothermal compressibility obtained from the compressibility route. This is done in thermodynamically self-consistent integral equation approaches, like e.g. the modified hypernetted-chain (MHNC) theory [34]. In this approach the OZ relation is solved with the closure relation

$$g(r) = e^{-\beta\phi(r)+h(r)-c(r)+E(r)}, \tag{4.6}$$

where the bridge function $E(r)$ is approximated by that of a suitably chosen HS reference system assuming the universality hypothesis of the bridge functions [34]. The $E(r)$ are either obtained from the Verlet-Weis parameterization of the pair distribution function or,

alternatively, by the PY bridge function. The HS diameter is chosen to enforce equality of the compressibility via the virial and the compressibility route (4.5).

Other thermodynamic self-consistent closure relations use so called 'mixed closure' relations, i.e. they interpolate in a functional form between two different conventional closure relations. In this interpolation scheme a mixing function $f_\alpha(r)$ with an adjustable parameter α is introduced that is chosen so that consistency is enforced. One of these approaches is the Rogers Young (RY) approximation [35] that interpolates between the PY and the HNC approximation. Its closure is given by

$$g(r) = e^{-\beta\phi(r)} \left(1 + \frac{e^{f_\alpha(r)[h(r)-c(r)]} - 1}{f_\alpha(r)}\right). \tag{4.7}$$

An appropriate form for f_α would be e.g. $f_\alpha(r) = 1 - e^{-\alpha r}$, i.e. for $r = 0$ the PY solution is obtained that is more appropriate for short-ranged forces, while in the limit $r \to \infty$ one obtains the HNC closure that is accurate for long-ranged potentials and uses the approximation that $E(r) = 0$. The RY approximation yields excellent results for purely repulsive systems.

Another self-consistent 'mixed closure' integral equation theory is the HMSA [36], that interpolates between the HNC and the SMSA and is more suitable for systems with attractive potential than the RY approximation. Its closure is given by

$$g(r) = e^{-\beta\phi_R(r)} \left(1 + \frac{e^{f_\alpha(r)[h(r)-c(r)-\phi_A(r)]} - 1}{f_\alpha(r)}\right), \tag{4.8}$$

where

$$\phi_R(r) = \begin{cases} \phi(r) - \phi(r_m) & r \le r_m \\ 0 & r > r_m \end{cases} \tag{4.9}$$

is the repulsive part of the potential and

$$\phi_A(r) = \begin{cases} \phi(r_m) & r \le r_m \\ \phi(r) & r > r_m \end{cases} \tag{4.10}$$

the attractive one; r_m denotes a suitably chosen separation distance, in general it is the position of the minimum of the potential. For the mixing function $f_\alpha(r)$ one can assume a function as the one used above. In both approaches the parameter α is varied until eq. (4.5) is satisfied.

The MHNC, GMSA, and HMSA yield accurate thermodynamics and predict accurately the liquid and vapor branches of the coexistence curves [37, 38], but they fail to converge close to the critical point, leaving the two branches unconnected [39] and estimates for the critical point parameters can only be obtained by extrapolation.

The two probably most promising approaches at the moment that circumvent these problems are the hierarchical reference theory (HRT) [7] and the thermodynamically self-consistent Ornstein Zernike approach (SCOZA) both of them providing very accurate predictions for the thermodynamics, the phase diagrams and the critical behavior. Especially in the critical region, where the accuracy of integral equation theories and perturbation theories decreases dramatically (they do not succeed in reproducing the shape of the coexistence curve and the location of the critical points correctly) or their solution fails, both theories remain highly accurate and successful.

The SCOZA was proposed already some time ago by Høye and Stell [40, 41], but it was only recently that it could be solved numerically for a model system and results of remarkable accuracy were obtained [8].

The theory has been formulated in different versions, all of them building directly upon the MSA closure and combining it with the requirement of thermodynamic consistency [6] thus removing the main deficiency of the MSA. In the different versions one or more state dependent functions are introduced in the MSA relation between $c(r)$ and $-\beta\phi(r)$; and this (or these) function(s) is (are) determined in such a way that thermodynamic consistency via different thermodynamic routes is ensured, thus leading to (a) partial differential equation(s) (PDE) for this (these) parameter(s). The various versions of the SCOZA differ in the choice of these adjustable parameters.

The most comprehensive concept of this theory proposed in [40, 41] ensures self-consistency between the virial, the energy as well as the compressibility route. Due to the complexity its numerical solution was implemented for a hard-core one-Yukawa fluid (HC1Y) only recently by Caccamo *et al.* [38]. (In their contribution this version of the SCOZA is actually called GMSA[1], while the designation SCOZA therein refers to another version of the SCOZA.) In this contribution the closure relation to the OZ equation is

$$\begin{aligned} g(r) &= 0 && \text{for} \quad r < \sigma \\ c(r) &= -\beta\phi(r) + K\frac{e^{-z(r-\sigma)}}{r} && \text{for} \quad r > \sigma, \end{aligned} \tag{4.11}$$

where σ is again the HC diameter and K and z are adjustable state-dependent parameters to ensure thermodynamic consistency. The numerical solution of this approximation was not obtained by solving a PDE but through an iterative procedure.

The version of the SCOZA with which we will be concerned in the following contains only one state dependent function $K(\rho, \beta)$ which appears as a proportionality factor

[1]The term GMSA comprises a family of approximations, all of which have the common feature of supplementing the $-\beta\phi(r)$ term in the direct correlation function with additional Yukawa terms. The amplitudes and ranges of these Yukawa terms are adjusted to yield thermodynamic self-consistency.

between $\phi(r)$ and the direct correlation function $c(r)$ outside the core, and enforces consistency only between the compressibility and the energy route. This closure relation amounts to setting

$$\begin{aligned} g(r) &= 0 && \text{for} \quad r < \sigma \\ c(r) &= K(\rho,\beta)\phi(r) && \text{for} \quad r > \sigma, \end{aligned} \tag{4.12}$$

where $K(\rho,\beta)$ is a function of the thermodynamic state (ρ,β). The condition on $g(r)$, the so-called core condition, is exact, while the expression for $c(r)$ is an approximation and implies that $c(r)$ has the same range as the potential - an ansatz that is usually referred to as the OZ approximation, thus the name self-consistent Ornstein Zernike approximation. In contrast to the MSA, where $K(\rho,\beta) = -\beta$, here $K(\rho,\beta)$ is not fixed a priori but is instead determined so that thermodynamic consistency is ensured between the compressibility and the energy route. The advantage of this simple recipe is that the solution of the OZ equation together with the closure relation (4.12) is the same as for the MSA problem.

This scheme of the SCOZA was already proposed in [41] where equations for solving the self-consistency problem were derived. Preliminary results for a three dimensional lattice gas for supercritical temperatures indicated that SCOZA could produce accurate results [42]. However, results were limited to supercritical temperatures since the numerical solution of the SCOZA PDE of [41] was found to be unstable when proceeding to temperatures below the critical point.

The first numerical results below T_c were obtained by Dickman and Stell for a three-dimensional nearest neighbor lattice gas [8]. In contrast to the original (numerically unstable) PDE used in [41], where the Helmholtz free energy was used as the quantity to solve for, these authors have used the following PDE as basis for the SCOZA equation: assuming that the thermodynamics stems from a unique Helmholtz free energy the consistency condition can be expressed as

$$\frac{\partial}{\partial\beta}\left(\frac{1}{\chi^{red}}\right) = \rho\frac{\partial^2 u}{\partial\rho^2}, \tag{4.13}$$

where $\chi^{red} = \rho k_B T \chi_T$ is the reduced isothermal compressibility given by the fluctuation theorem and $u = \frac{U^{ex}}{V}$ is the excess (over ideal) internal energy per volume given by the energy equation. Eq. (4.13) supplemented by the closure relation eq. (4.12) and the OZ relation yields a PDE for $K(\rho,\beta)$. Using the analytic structure of the solution of the OZ equation with the closure relation (4.12) for the system they investigated, Dickman and Stell were able to express $1/\chi^{red}$ in closed form in terms of u and to derive a PDE of diffusion type for $1/\chi^{red}$. The numerical solution procedure of this PDE was refined

in subsequent work by Pini *et al.* [43]. Pini developed an unconditionally, accurate and efficient solution algorithm, using his experience from previous work on the HRT: although this theory, that is based on renormalization group, is conceptually different from the SCOZA (for an overview see [7]), it also results in the numerical problem of solving a non-linear PDE of diffusion type.

In [8] Dickman and Stell considered the lattice gas (or the equivalent Ising model) in three dimensions with nearest neighbor interactions on various cubic lattices. The predictions were remarkably accurate, e.g. the values of T_c were obtained within 0.2% of best estimates and other critical properties agreed within 1-2% of the best numerical estimates. Also the various effective critical exponents, that are defined as the slopes of curves of logarithmic plots, e.g.

$$\gamma^{\text{eff}} = \frac{d \log \chi_T^{-1}}{d \log t}, \tag{4.14}$$

where $t = \frac{T - T_c}{T_c}$, were investigated, and it was found that they were close to the estimated exact form unless very close to the critical point. Further numerical results for the three-dimensional lattice gas by Borge and Høye [44] and Pini *et al.* [43] confirmed this picture: above the critical temperature the theory yields the same critical exponents as the spherical model but this regime is very narrow, so that thermodynamics and effective exponents are in good agreement with the true critical behavior until the temperature differs from its critical value by less than 1%. On the coexistence curve (i.e. below T_c), on the other hand, the exponents are neither spherical nor classical and turn out to be very accurate: e.g. the curvature of the coexistence curve is described by $\beta = 0.35$ which is near to the exact value of $\beta \sim 0.326$ [45]. Borge and Høye [44] also investigated the influence of the interaction range and they found that the effective critical exponents away from the critical point vary with this range.

An analytic study of the SCOZA critical exponents and the scaling behavior in three dimensions was given by Høye *et al.* [46]. It was seen that standard scaling is not fulfilled, but rather a generalized form of scaling. In this study the SCOZA subcritical exponents for a three-dimensional system were determined to be

$$\beta = 7/20, \gamma = 7/5, \alpha = -1/10, \tag{4.15}$$

which are in remarkable agreement with the exact values $\beta \sim 0.326, \gamma \sim 1.24, \alpha \sim 0.11$ [45], despite the fact that SCOZA does not incorporate renormalization group ideas. On the other hand, the supercritical exponents are spherical ones

$$\gamma = 2, \delta = 5, \alpha = 0, \tag{4.16}$$

so the indices above do not fulfill the standard scaling relations. Thus, SCOZA fails in a very narrow regime of $|t| < 10^{-3}$ in the vicinity of the critical point which is also the error in T_c for the Ising model. However, outside this region results turn out to be very accurate.

After the first applications of the SCOZA to lattice systems, it was extended subsequently to continuum systems, too [47, 48, 49, 50]. In particular, in the case when u in eq. (4.13) can be written in closed form as a function of χ^{red} within the closure relation (4.12) the numerical solution of the SCOZA is substantially simplified leading to a PDE for u. This is actually the case for the HCY fluid, where one can make use of the extensive semi-analytic MSA studies available. So it is not surprising that the SCOZA for continuum fluids has been solved initially only for the hard-core 1-Yukawa (HC1Y) [47, 48] and hard-core 2-Yukawa (HC2Y) fluid [49, 50]. The general case has to be solved fully numerically.

In [47] the accuracy of the SCOZA approach remained somewhat unclear due to the uncertainty of the available simulation results. But it was already seen that the top of the coexistence curve was flattening, having a shape that is similar to the one of real fluids. In this paper the closure relation of eq. (4.12) was used, implying that the HS contribution to $c(r)$ vanishes outside the core, so that the treatment of the HS reference system coincides with the Percus-Yevick approximation. Alternatively, these authors also incorporated a more accurate HS theory by using a Yukawa tail that is non zero at $\beta = 0$ to reproduce the CS equation of state.

In subsequent work [48] the treatment of the HS reference part was improved by adding to $c(r)$ in (4.12) a non-vanishing contribution $c_{\rm HS}(r)$ outside the core. However, the Verlet-Weis parameterization [51] of $c_{\rm HS}(r)$, which is the most popular parameterization for the HS structure functions reproducing with high accuracy simulation data, is not convenient for the formulation of the analytic part of the SCOZA. Instead the Waisman parameterization was used, where the function $c_{\rm HS}(r)$ outside the core is assumed to have a one-Yukawa form

$$\begin{aligned} g(r) &= 0 && \text{for} \quad r < \sigma \\ c(r) &= K(\rho,\beta)\phi(r) + K_{\rm HS}\frac{e^{-z_{\rm HS}(r-\sigma)}}{r} && \text{for} \quad r > \sigma; \end{aligned} \tag{4.17}$$

the amplitude $K_{\rm HS}$ and range $z_{\rm HS}$ are determined in such a way to reproduce CS thermodynamics. The reason why one chooses the Waisman parameterization for the HS part of the direct correlation function is a purely technical one: the mathematical formulation of the SCOZA for a $c(r)$ of 2-Yukawa form is still convenient since analytic studies for the case when $c(r)$ is a linear combination of two Yukawas [32, 52, 41] are available.

These two approaches for the HS part - the two Yukawa $c(r)$ and the one Yukawa $c(r)$ that reproduces CS behavior at $\beta = 0$ - were found to make little difference. In [48] also a new set of simulations was performed to check the SCOZA results and again the accuracy of the thermodynamics, the critical data and the coexistence curve was remarkable: the critical temperature and density predicted by SCOZA agreed with simulation results to about 0.6 %. Another application of the 2-Yukawa version of the SCOZA is to take both Yukawa terms to represent the interaction. This was actually done in order to parameterize a Lennard Jones (LJ) fluid mimicked by a hard-core two Yukawa interaction [49] and, furthermore, to investigate the effect of competing interactions on the liquid-vapor transition [50]. In the latter study the 2-Yukawa tail was assumed to be attractive at short distance and repulsive at long distance.

Since results for the three-dimensional lattice gas and the HC Yukawa fluid have confirmed that the SCOZA remains highly accurate even in the critical region, it was of interest to develop the SCOZA for other fluid and lattice gas systems and to test its general accuracy more precisely in various situations. Work in this direction has been done: the formulation of the SCOZA has been generalized to D-dimensional and continuous spins [53] and first numerical results were produced [54]. As a further test of its accuracy the SCOZA was compared with exact results for the Ising model in one and two dimension [55, 56]. In the latter case comparison with the exact Onsager solution in zero magnetic field with nearest neighbor interaction was made. A special feature in this case is that SCOZA as the MSA does not give a true phase transition in two dimensions, i.e. the singularities are smeared out. This deficiency of the SCOZA is due to the Ornstein Zernike ansatz which does not include a long-range part of the direct correlation function that would be necessary in the critical region. According to this approximation the critical exponent η is found to be 0 instead of the exact value of $\eta \sim 0.006$ in three dimensions; thus the behavior of the total correlation function is distorted which decays as $h(r) \sim f(r/\xi)/r^{d-2+\eta}$ for $r \gg 1$, where d is the dimension and ξ the correlation length. However this deficiency is only crucial in the vicinity of the critical point, where $f(r/\xi)$ is constant rather than exponentially decaying. Despite this deficiency, also in the two-dimensional case numerical results were again convincing. The temperature where the specific heat has a maximum was found almost precisely at the exact critical point temperature. Since SCOZA treats the infinite system as if it were a finite one, comparison with finite-sized simulation were done [56].

Good results have also been obtained when generalizing the SCOZA to a disordered system like the site diluted random field Ising model [57], and it has recently been applied to the spin-1 model [58] and the q-state Potts model [59]. Furthermore a binary mixture

model has been studied within the SCOZA by A. Dickman and Stell [60]: the decorated model, that is isomorphic to the lattice gas model.

Initially, in the case of continuum fluids, applications of the SCOZA were restricted to the one-component case and to hard-core (HC) interactions with one or two Yukawa tails (with the possibility of approximating a Lennard-Jones potential rather accurately [49])) since the initial formulation was based on the semianalytic MSA solution via the Laplace transform route (see below). In subsequent work when the SCOZA was reformulated on the bases of the more elegant and more flexible Wertheim-Baxter factorization technique [61, 62] a broader applicability of the theory came within reach including now all systems for which the semi-analytic Blum-Høye MSA solution is available. So it became possible to extend the SCOZA to HC systems with a formally arbitrary number of Yukawa tails [63]. As a test system the model fullerenes $C_{60} - C_{96}$ described via an approximation of the sphericalized Girifalco potential through a suitable linear combination of Yukawa tails were investigated [63, 64, 65]. In particular, C_{60} has become of great interest in the last years (for an overview see [37]) because the pair potential differs significantly from the LJ one: the ratio of the width of the attractive well to the equilibrium distance is much less for the C_{60}-C_{60} intermolecular potential than for the LJ one, furthermore the repulsive wall of the C_{60}-C_{60} interaction is much stiffer. Since the phase behavior depends in a very sensitive way on the nature of the forces the phase behavior was expected to be completely different from that of rare gas atoms. It was even speculated that C_{60} might be a substance with no liquid phase at all. The SCOZA, being known to yield reliable and accurate results for the coexistence curves even in the critical regions, confirmed that C_{60} should possess a liquid phase. Comparison with previous simulation results illustrated once more that the SCOZA yields reliable predictions even in the critical region. In [63] also the phase behaviour of a HC system with an explicitly density-dependent attractive Yukawa tail (introduced via a density-dependent inverse screening length) was studied and, for a particular form of the density dependence, the phenomenon of double criticality observed, i.e. two first-order phase transitions (liquid-vapour and liquid-liquid) each with its own critical point. Furthermore the SCOZA was extended to binary symmetric mixtures of HC Yukawa systems [66, 67].

The purpose of the work presented here is to extend the SCOZA to a larger class of continuum fluids. First, we have generalized the SCOZA to a one-component fluid with a hard-core and a linear combination of Sogami-Ise tails [68]. The theoretical formulation is given in section 4.3. The advantage of this generalization is the opportunity that any smooth realistic interaction can be approximated very accurately by a linear combination of Sogami-Ise tails. In section 4.4 the theory is applied to study the thermo-

dynamic properties and the phase behavior of various model systems and a comparison with LOGA/ORPA results is made. We further use the SCOZA to study binary symmetric mixtures with long-ranged Yukawa interactions. Details of the semi-analytic MSA results on which the SCOZA formulation is based are summarized in Appendices A, B, and C.

4.2 SCOZA for a One-Component Fluid

In our investigations we have chosen the version of the SCOZA proposed recently by Pini *et al.* [48] given by the closure relation eq. (4.17). For the interaction between the particles these authors have chosen a hard-core Yukawa (HCY) pair potential which has been of interest in the last years [37, 38] due to several reasons: *first*, for this simple model one has available semi-analytic theories [30, 69, 32, 52, 41, 14]. Thus the formulation of the MSA, the GMSA and the SCOZA is particularly simplified for the HCY fluid. This is not the case for other pair potentials like the square well fluid where the solution has to be obtained fully numerically. *Second*, this simple potential comprises the two key features that mimic a more realistic potential: a highly repulsive core and an attractive tail. The latter is required to observe first order liquid-gas phase transitions and liquid-gas criticality. *Third*, the potential parameters can be chosen so as to provide more realistic potentials like a solvent-averaged interaction potential between poly-electric or colloidal particles. Furthermore, the HCY potential comprises as special limiting cases the adhesive HS system [17] (when the Yukawa tail is infinitely deep and the screening length infinitely large) and charged HSs (when the screening length z is set to 0).

However, the HCY potential fails to mimic realistic interactions, the strength of the attractive tail being largest at the infinitely high hard-core repulsion. The Sogami-Ise interaction on the other hand represents a smoother, more realistic potential, and retains the mathematical conveniences of the HCY fluid. However, compared to the HCY fluid the formalulation of the SCOZA is now more complex and cumbersome.

The OZ equation along with the MSA closure for a HC-Yukawa system (i.e., the core condition for the pair distribution function and a direct correlation function that is of Yukawa form outside the core) has been solved semi-analytically via two different approaches. Waisman [30] has used the so called Laplace transform technique [61]. His solution for a one-Yukawa form of $c(r)$ was simplified in subsequent work [69] and generalized to the case when $c(r)$ is a linear combination of two Yukawas by Høye and Stell [32, 52, 41]. The other approach was introduced by Høye and Blum [14]. It ap-

plies a method of Baxter [62] which is based on the Wiener-Hopf factorization of the Fourier transforms of the direct correlation functions by introducing so called factor functions. In this approach the generalization of the solution from a one-Yukawa tail to the multi-Yukawa form of the direct correlation function and to multi-component systems is straightforward and considerably easier than for the Laplace transform route. Recently this semi-analytic approach has also been generalized by Yasutomi and Ginoza [70] to multi-component fluids with a Sogami-Ise [71] type closure relation and to fluid mixtures with screened Coulomb plus power series interactions [72, 73, 74, 75].

While the formulation of the SCOZA for a one and two-Yukawa fluid presented in [47, 48, 49] is based on the first approach, the latter approach brings a larger variety of model systems, that can be studied with SCOZA, within reach: the one-component multi-Yukawa fluid, the one-component multi-Sogami-Ise fluid, and the multi-component HC Yukawa system. In their analysis of the HC Yukawa fluid Høye and Blum reformulated the problem as a system of nonlinear equations for the coefficients of the factor functions. For the more general case of multi-component, multi-Yukawa fluid mixtures Arrieta *et al.* [76] have cast these equations into a form suitable and more convenient for numerical calculations and provided a general, direct solution algorithm. Yasutomi and Ginoza [70] have extended Blum-Høye's work in a straightforward way to systems with Sogami-Ise pair potentials; we have generalized Arrieta's work to these systems, i.e. we reformulated the nonlinear equations in a form that is suitable for the numerical calculations and found a stable solution algorithm; the set of the nonlinear equations and their coefficients are summarized in Appendices A, B. At the beginning we briefly summarize the analytic MSA results relevant for our formulation of the SCOZA.

4.3 Formulation of the Theory

We consider a fluid of particles interacting via a spherically symmetric Sogami-Ise type pair potential $\phi(r)$ given by

$$\phi(r) = \begin{cases} +\infty & r \leq \sigma \\ w(r) & r > \sigma \end{cases}, \tag{4.18}$$

where the repulsion is characterized by the hard-sphere diameter σ and the attractive tail $w(r)$ is given by a linear combination of a Coulomb potential plus a constant that are both screened with an exponential

$$w(r) = -\epsilon\sigma \sum_{\nu=2}^{n} \left(\frac{K_\nu}{r} + L_\nu z_\nu \right) e^{-z_\nu (r-\sigma)}. \tag{4.19}$$

The z_ν are the screening lengths, the K_ν and L_ν are the coefficients of the linear combination and chosen so that the minimum of the function $-\sigma \sum_{\nu=2}^{n} \left(\frac{K_\nu}{r} + L_\nu z_\nu\right) e^{-z_\nu(r-\sigma)}$ on the interval $[\sigma, \infty)$ is -1, and ϵ is the depth of the potential. Greek indices are used to designate the different Sogami-Ise tails and summations - unless otherwise stated - will be extended over n tails. Here the summation starts at $\nu = 2$ since the first Sogami-Ise tail is reserved for the description of the HC reference system (see below).

The version of the SCOZA considered here [48] is based on the OZ equation

$$h(r) = c(r) + \rho \int d^3r' c(r')\, h(|\mathbf{r} - \mathbf{r}'|) \tag{4.20}$$

supplemented with the following closure relation

$$\begin{aligned} g(r) &= 0 && \text{for} \quad r \leq \sigma \\ c(r) &= c_{\text{HS}}(r) + K(\rho,\beta) w(r) && \text{for} \quad r > \sigma. \end{aligned} \tag{4.21}$$

$h(r)$ and $c(r)$ are the total and direct correlation functions, $g(r) = h(r) - 1$ is the pair distribution function, $c_{\text{HS}}(r)$ is the direct correlation function of the hard-sphere (HS) reference system and $K(\rho, \beta)$ is a yet undetermined function depending on the thermodynamic state that is given by the density ρ and the inverse temperature $\beta = 1/k_B T$, k_B being the Boltzmann constant. The closure resembles to the one used in the LOGA/ORPA) [20, 21] where $K(\rho, \beta) = -\beta$ is fixed. Here, $K(\rho, \beta)$ is not given *a priori* but is determined so that thermodynamic self-consistency is guaranteed between the compressibility and the energy route to the thermodynamic properties.

We recall that, according to the compressibility route the reduced isothermal compressibility via the compressibility route is given by

$$\frac{1}{\chi^{red}} = \frac{\partial \beta P}{\partial \rho} = 1 - \rho \tilde{c}(k = 0), \tag{4.22}$$

where $\tilde{c}(k)$ denotes the Fourier transform of $c(r)$

$$\tilde{c}(k) = \int c(r) e^{-i\mathbf{kr}} d^3r. \tag{4.23}$$

On the other hand the excess (over ideal) internal energy per unit volume calculated via the internal energy route is

$$\frac{U^{ex}}{V} = u = 2\pi\rho^2 \int_\sigma^\infty dr r^2 w(r) g(r). \tag{4.24}$$

If χ^{red} and u are consistent with each other, they must stem from a unique Helmholtz free energy density $\frac{F}{V} = f = f^{id} + f^{ex}$, where f^{id} and f^{ex} are the ideal and excess parts of the free energy density. Thus

$$\rho \frac{\partial^2 u}{\partial \rho^2} = \rho \frac{\partial^2}{\partial \rho^2} \frac{\partial \beta f^{ex}}{\partial \beta} = \frac{\partial}{\partial \beta} \left(\rho \frac{\partial \beta \mu^{ex}}{\partial \rho} \right) = \frac{\partial}{\partial \beta} \left(\frac{1}{\chi^{red}} \right), \tag{4.25}$$

where $\mu^{ex} = \frac{\partial f^{ex}}{\partial \rho}$ is the excess chemical potential. For approximate $g(r)$ as obtained, for instance, by conventional integral equation and perturbation theories [4], eq. (4.25) where χ^{red} is given by eq. (4.22) and u by eq. (4.24) is not fulfilled. In the SCOZA, however, this consistency is enforced through an appropriate choice of the yet undetermined function $K(\rho, \beta)$ that is obtained by solving the partial differential equation (PDE) eq. (4.25) supplemented by eqs. (4.20), (4.21), (4.22), and (4.24). The solution of the SCOZA PDE is simplified by making use of the semi-analytic solution of the MSA for Sogami-Ise type potentials [70] that allows one to express χ^{red} as a function of u thus transforming the PDE (4.25) into a PDE for u. This will be outlined in the following. So we start by briefly summarizing the semi-analytic solution of the MSA.

Following Baxter's factorization method it can be shown that under certain conditions [77] the OZ relation is equivalent to the equations

$$\begin{aligned} 2\pi r c(r) &= -Q'(r) + \rho \int_0^\infty Q(t) Q'(r+t) dt \\ 2\pi r h(r) &= -Q'(r) + 2\pi\rho \int_0^\infty (r-t) h(|r-t|) Q(t) dt, \end{aligned} \tag{4.26}$$

where the factor function $Q(r)$ has been introduced. From eqs. (4.26) and from the closure relation

$$\begin{aligned} h(r) &= -1 && r \le \sigma \\ c(r) &= \sum \left(\frac{\widetilde{K}_\nu}{r} + \widetilde{L}_\nu z_\nu \right) e^{-z_\nu (r-\sigma)} && r > \sigma, \end{aligned} \tag{4.27}$$

it follows [70] that $Q(r)$ must have the form

$$Q(r) = Q^0(r) + \sum \frac{1}{z_\nu} \left(D_\nu + E_\nu z_\nu r \right) e^{-z_\nu (r-\sigma)}, \tag{4.28}$$

where

$$Q^0(r) = \begin{cases} \frac{a}{2}(r-\sigma)^2 + b(r-\sigma) + \sum \frac{1}{z_\nu} \left(C_\nu + F_\nu \right) \left(e^{-z_\nu (r-\sigma)} - 1 \right) \\ \qquad + \sum F_\nu \left(r e^{-z_\nu (r-\sigma)} - \sigma \right) & 0 < r < \sigma \\ 0 & \text{otherwise} \end{cases}, \tag{4.29}$$

with yet undetermined coefficients $a, b, C_\nu, D_\nu, E_\nu$ and F_ν.

One further introduces the quantities

$$G_\nu = z_\nu \hat{g}(z_\nu) e^{z_\nu \sigma} = z_\nu \int_\sigma^\infty r e^{-z_\nu (r-\sigma)} g(r) dr, \tag{4.30}$$

and

$$G_\nu^{(1)} = z_\nu \hat{g}^{(1)}(z_\nu) e^{z_\nu \sigma} = z_\nu \int_\sigma^\infty r^2 e^{-z_\nu (r-\sigma)} g(r) dr, \tag{4.31}$$

where $\hat{g}(z)$ and $\hat{g}^{(1)}(z)$ denote the Laplace transforms of $rg(r)$ and $r^2g(r)$. The use of G_ν and $G_\nu^{(1)}$ instead of $\hat{g}(z_\nu)$ and $\hat{g}^{(1)}(z_\nu)$ follows the procedure adopted for the HS Yukawa system [78, 76] and is due to numerical reasons since it allows one to reduce the number of evaluations of exponentials when calculating the coefficients of equations (A.1)-(A.4). Especially, expressions with positive exponentials are avoided. Inserting the form of $Q(r)$ in eqs. (4.26) and using the closure relation (4.27) allows one to express the unknown variables a, b, C_ν, and F_ν as functions of D_ν, E_ν, G_ν, and $G_\nu^{(1)}$ and to derive a system of $4n$ nonlinear equations for the $4n$ unknowns D_ν, E_ν, G_ν, and $G_\nu^{(1)}$. This procedure is a direct extension of Blum and Høye's work for HS Yukawa systems [79] and is explained in detail by Yasutomi and Ginoza [70]. This system of $4n$ nonlinear equations can be divided into 4 subsets of n equations. We have cast them into a form suitable for numerical integration and compiled them in Appendix A.

All energy-related quantities ϵ and β enter the eqs. (A.1)- (A.4) only via

$$A_\nu^{(7)} = 2\pi\widetilde{L}_\nu, \quad \forall\nu \tag{4.32}$$

and

$$C_\nu^{(13)} = 2\pi\widetilde{K}_\nu, \quad \forall\nu \tag{4.33}$$

while the remaining coefficients are temperature independent. Their explicit expressions are given in Appendix B. They are calculated from the system parameters ρ, z_ν, and σ.

Equations (A.3) and (A.4) are linear in D_ν and E_ν for given G_ν and $G_\nu^{(1)}$ and can be rewritten as

$$\begin{aligned} \sum_{\tau=1}^{n} O_{\nu\tau}D_\tau + \sum_{\tau=1}^{n} P_{\nu\tau}E_\tau &= Q_\nu \\ \sum_{\tau=1}^{n} R_{\nu\tau}D_\tau + \sum_{\tau=1}^{n} S_{\nu\tau}E_\tau &= T_\nu. \end{aligned} \tag{4.34}$$

The definitions of the coefficients of eqs. (4.34) are compiled in Appendix A. Solution of this system of $2n$ linear equations yields D_ν and E_ν as functions of ρ, G_ν and $G_\nu^{(1)}$. This result can then be inserted into eqs. (A.1) and (A.2) which become a set of $2n$ coupled nonlinear equations in the G_ν and $G_\nu^{(1)}$.

Once the D_ν, E_ν, G_ν, and $G_\nu^{(1)}$ are known, thermodynamic properties can be determined as follows. The inverse reduced isothermal compressibility calculated via the fluctuation theorem is found to be

$$\frac{1}{\chi^{red}} = 1 - \rho\tilde{c}(k=0) = \left(\frac{a}{2\pi}\right)^2. \tag{4.35}$$

The expression for a in terms of the quantities $G_\nu, G_\nu^{(1)}, D_\nu$, and E_ν is obtained from

$$a = A^0(1+M) - \frac{4}{\sigma^2}B^0 N \tag{4.36}$$

with

$$\begin{aligned} M &= -\rho\sum_{\tau=1}^{n}\left[\left(\frac{M_\tau^{(a)}}{z_\tau^2} - 2\pi\rho\frac{G_\tau}{z_\tau^4}(M_\tau^{(a)}e^{-z_\tau\sigma}-1)\right)D_\tau\right. \\ &\quad \left.+\left(\frac{P_\tau^{(a)}}{z_\tau^2} - 2\pi\rho\frac{G_\tau}{z_\tau^4}(2L_\tau^{(a)}e^{-z_\tau\sigma}-2) - 2\pi\rho\frac{G_\tau^{(1)}}{z_\tau^3}(M_\tau^{(a)}e^{-z_\tau\sigma}-1)\right)E_\tau\right] \\ N &= \rho\sum_{\tau=1}^{n}\left[\left(\frac{L_\tau^{(a)}}{z_\tau^3} - 2\pi\rho\frac{G_\tau}{z_\tau^5}(L_\tau^{(a)}e^{-z_\tau\sigma}-1)\right)D_\tau\right. \\ &\quad \left.+\left(\frac{2Q_\tau^{(a)}}{z_\tau^3} - 2\pi\rho\frac{G_\tau}{z_\tau^5}(3O_\tau^{(a)}e^{-z_\tau\sigma}-3) - 2\pi\rho\frac{G_\tau^{(1)}}{z_\tau^4}(L_\tau^{(a)}e^{-z_\tau\sigma}-1)\right)E_\tau\right]; \end{aligned} \tag{4.37}$$

the quantities $M_\tau^{(a)}, P_\tau^{(a)}, L_\tau^{(a)}, Q_\tau^{(a)}, O_\tau^{(a)}, A^0$, and B^0 are again calculated from ρ, z_ν, and σ; the respective expressions are compiled in Appendix B.

The excess internal energy per unit volume calculated via the internal energy route is found to be

$$u = -2\pi\rho^2\epsilon\sigma\sum_{\nu=2}^{n}\left(\frac{K_\nu}{z_\nu}G_\nu + L_\nu G_\nu^{(1)}\right). \tag{4.38}$$

Now we have summarized the semi-analytic MSA results relevant for SCOZA and we proceed with the formulation of the SCOZA. In order to stay within the framework of the Sogami-Ise type closure we choose the Waisman parameterization for $c_{\rm HS}(r)$ [30, 69] which ensures a highly self-consistent description of the thermodynamic properties of the HS part. It assumes a Yukawa form for $c_{\rm HS}(r)$ outside the hard-core

$$c_{\rm HS}(r) = K_1(\rho)\frac{e^{-z_1(\rho)(r-\sigma)}}{r} \quad \text{for} \quad r > \sigma \tag{4.39}$$

where $K_1(\rho)$ and $z_1(\rho)$ are known functions of the density (see Appendix A of [48]). These expressions guarantee that both compressibility and virial route yield the Carnahan Starling (CS) equation of state [31] for the HS reference system. Using eqs. (4.19) and (4.39), relation (4.21) becomes

$$\begin{aligned} g(r) &= 0 && \text{for} \quad r \le \sigma \\ c(r) &= K_1(\rho)\tfrac{e^{-z_1(\rho)(r-\sigma)}}{r} - K(\rho,\beta)\epsilon\sigma\textstyle\sum_{\nu=2}^{n}\left(\frac{K_\nu}{r} + L_\nu z_\nu\right)e^{-z_\nu(r-\sigma)} && \text{for} \quad r > \sigma. \end{aligned} \tag{4.40}$$

We use now the analytic results presented above to derive a relation between χ^{red} and u, leading to a PDE for u. Using eq. (4.35), the consistency relation (4.25) reads

$$2\frac{a}{(2\pi)^2}\frac{\partial a}{\partial u}\frac{\partial u}{\partial \beta} = \rho\frac{\partial^2 u}{\partial \rho^2}. \tag{4.41}$$

a is given by eqs. (4.36), (4.37) as a function of D_ν, E_ν, G_ν, and $G_\nu^{(1)}$; inserting the solutions $D_\nu(\rho, G_\nu, G_\nu^{(1)})$ and $E_\nu(\rho, G_\nu, G_\nu^{(1)})$ of the linear system eq. (4.34) in eqs. (4.36) and (4.37) yields $a(\rho, G_\nu, G_\nu^{(1)})$ and thus

$$2\frac{a}{(2\pi)^2}\sum_{\nu=1}^{n}\left(\frac{\partial a}{\partial G_\nu}\frac{\partial G_\nu}{\partial u} + \frac{\partial a}{\partial G_\nu^{(1)}}\frac{\partial G_\nu^{(1)}}{\partial u}\right)\frac{\partial u}{\partial \beta} = \rho\frac{\partial^2 u}{\partial \rho^2} \tag{4.42}$$

or

$$B(\rho, u)\frac{\partial u}{\partial \beta} = \rho\frac{\partial^2 u}{\partial \rho^2}, \tag{4.43}$$

once that a, $\frac{\partial a}{\partial G_\nu}$, $\frac{\partial a}{\partial G_\nu^{(1)}}$, $\frac{\partial G_\nu}{\partial u}$, and $\frac{\partial G_\nu^{(1)}}{\partial u}$ have been determined as functions of ρ and u (see below). $B(\rho, u)$ is given by

$$B(\rho, u) = 2\frac{a}{(2\pi)^2}\sum_{\nu=1}^{n}\left(\frac{\partial a}{\partial G_\nu}\frac{\partial G_\nu}{\partial u} + \frac{\partial a}{\partial G_\nu^{(1)}}\frac{\partial G_\nu^{(1)}}{\partial u}\right) \tag{4.44}$$

Thus we now have derived a PDE for $u(\rho, \beta)$.

What remains is to determine a, $\frac{\partial a}{\partial G_\nu}$, $\frac{\partial a}{\partial G_\nu^{(1)}}$, $\frac{\partial G_\nu}{\partial u}$, and $\frac{\partial G_\nu^{(1)}}{\partial u}$ as functions of ρ and u. First of all we introduce $2n$ nonlinear equations $F_i(\rho, u, G_\nu, G_\nu^{(1)}) = 0,\ i = 1, \ldots, 2n$; their solution gives $G_\nu(\rho, u)$ and $G_\nu^{(1)}(\rho, u)$. The first equation is linear and is the energy equation (4.38)

$$u + 2\pi\rho^2\epsilon\sigma\sum_{\nu=2}^{n}\left(\frac{K_\nu}{z_\nu}G_\nu + L_\nu G_\nu^{(1)}\right) = 0 \tag{4.45}$$

or formally written as

$$F_1(\rho, u, G_2, \ldots, G_n, G_2^{(1)}, \ldots, G_n^{(1)}) = 0. \tag{4.46}$$

To establish the remaining $2n-1$ nonlinear equations we make use of eqs. (A.1) – (A.4) and eqs. (4.32),(4.33). Expressions for the $\widetilde{K}_\nu$ and $\widetilde{L}_\nu$ in eqs. (4.32),(4.33) are obtained by comparison of eq. (4.27) with the closure relation (4.40)

$$\begin{aligned}
\widetilde{K}_1 &= K_1(\rho) \\
\widetilde{L}_1 &= 0 \\
\widetilde{K}_\nu &= -K(\rho, \beta)\epsilon\sigma K_\nu \quad \text{for} \quad \nu = 2, \ldots, n \\
\widetilde{L}_\nu &= -K(\rho, \beta)\epsilon\sigma L_\nu \quad \text{for} \quad \nu = 2, \ldots, n
\end{aligned} \tag{4.47}$$

and thus

$$A_1^{(7)} = 0 \tag{4.48}$$

$$C_1^{(13)} = 2\pi K_1(\rho) \tag{4.49}$$

$$A_\nu^{(7)} L_\mu = A_\mu^{(7)} L_\nu \quad \text{for} \quad \nu, \mu = 2, \ldots, n \tag{4.50}$$

$$C_\nu^{(13)} K_\mu = C_\mu^{(13)} K_\nu \quad \text{for} \quad \nu, \mu = 2, \ldots, n \tag{4.51}$$

$$A_\mu^{(7)} K_\mu = C_\mu^{(13)} L_\mu \quad \text{for} \quad \mu = 2, \ldots, n. \tag{4.52}$$

The second nonlinear equation is eq. (A.1) for $\nu = 1$ where the solution $D_\nu(\rho, G_\nu, G_\nu^{(1)})$ and $E_\nu(\rho, G_\nu, G_\nu^{(1)})$ of eq. (4.34) and the relation (4.48) are inserted

$$\begin{aligned} E_1 \sum_{\tau=1}^{n} A_{\tau 1}^{(1)} G_\tau^{(1)} E_\tau + E_1 \sum_{\tau=1}^{n} A_{\tau 1}^{(2)} G_\tau E_\tau + E_1 \sum_{\tau=1}^{n} A_{\tau 1}^{(3)} G_\tau D_\tau \\ + E_1 \sum_{\tau=1}^{n} A_{\tau 1}^{(4)} E_\tau + E_1 \sum_{\tau=1}^{n} A_{\tau 1}^{(5)} D_\tau + E_1 A_1^{(6)} = 0 \end{aligned} \tag{4.53}$$

or, formally written as

$$F_2(\rho, G_\nu, G_\nu^{(1)}) = 0. \tag{4.54}$$

The third equation is eq. (A.2) for $\nu = 1$ where the solution $D_\nu(\rho, G_\nu, G_\nu^{(1)})$ and $E_\nu(\rho, G_\nu, G_\nu^{(1)})$ of eq. (4.34) and the relation (4.49) are inserted. The fourth equation corresponds to the eq. (4.52) for $\mu = 2$ using eqs. (A.1) and (A.2), i.e.

$$\begin{aligned} & K_2 \left(E_2 \sum_{\tau=1}^{n} A_{\tau 2}^{(1)} G_\tau^{(1)} E_\tau + E_2 \sum_{\tau=1}^{n} A_{\tau 2}^{(2)} G_\tau E_\tau + E_2 \sum_{\tau=1}^{n} A_{\tau 2}^{(3)} G_\tau D_\tau \right. \\ & \qquad \left. + E_2 \sum_{\tau=1}^{n} A_{\tau 2}^{(4)} E_\tau + E_2 \sum_{\tau=1}^{n} A_{\tau 2}^{(5)} D_\tau + E_2 A_2^{(6)} \right) \\ & - L_2 \left(E_2 \sum_{\tau=1}^{n} C_{\tau 2}^{(1)} G_\tau^{(1)} E_\tau + D_2 \sum_{\tau=1}^{n} C_{\tau 2}^{(2)} G_\tau^{(1)} E_\tau + E_2 \sum_{\tau=1}^{n} C_{\tau 2}^{(3)} G_\tau E_\tau \right. \\ & \qquad + D_2 \sum_{\tau=1}^{n} C_{\tau 2}^{(4)} G_\tau E_\tau + E_2 \sum_{\tau=1}^{n} C_{\tau 2}^{(5)} G_\tau D_\tau + D_2 \sum_{\tau=1}^{n} C_{\tau 2}^{(6)} G_\tau D_\tau \\ & \qquad + E_2 \sum_{\tau=1}^{n} C_{\tau 2}^{(7)} E_\tau + D_2 \sum_{\tau=1}^{n} C_{\tau 2}^{(8)} E_\tau + E_2 \sum_{\tau=1}^{n} C_{\tau 2}^{(9)} D_\tau \\ & \qquad \left. + D_2 \sum_{\tau=1}^{n} C_{\tau 2}^{(10)} D_\tau + E_2 C_2^{(11)} + D_2 C_2^{(12)} \right) = 0. \end{aligned} \tag{4.55}$$

The remaining $2n-4$ equations are obtained from eqs. (A.1), (A.3) for $\nu > 1$, inserting $D_\nu(\rho, G_\nu, G_\nu^{(1)})$ and $E_\nu(\rho, G_\nu, G_\nu^{(1)})$, the solution of eq. (4.34) and eliminating the unknown function $K(\rho, \beta)$ in the coefficients $A_\nu^{(7)}, C_\nu^{(13)}$ via the relations (4.50), (4.51) (for $\nu = 2, \mu =$

$3, \ldots, n$), formally written as

$$\begin{aligned} F_5(\rho, G_\nu, G_\nu^{(1)}) &= 0 \\ &\vdots \\ F_{2n}(\rho, G_\nu, G_\nu^{(1)}) &= 0. \end{aligned} \tag{4.56}$$

For given ρ and u the G_ν and $G_\nu^{(1)}$ are determined in the following way: the coupled set of nonlinear equations (4.46), (4.54)- (4.56) is solved numerically via a Newton-Raphson technique using explicit expressions for the Jacobian matrix $J = \left(\frac{\partial F_\mu}{\partial G_\nu}\right)$. In each step of the iteration the D_ν and E_ν are obtained by numerical solution of the linear system (4.34).

The analytic Jacobian matrix J is given by

$$J = \begin{pmatrix} 0 & 2\pi\rho^2\epsilon\sigma\frac{K_2}{z_2} & \ldots & 2\pi\rho^2\epsilon\sigma\frac{K_n}{z_n} & 0 & 2\pi\rho^2\epsilon\sigma L_2 & \ldots & 2\pi\rho^2\epsilon\sigma L_n \\ \frac{\partial F_2}{\partial G_1} & \frac{\partial F_2}{\partial G_2} & \cdots & \frac{\partial F_2}{\partial G_n} & \frac{\partial F_2}{\partial G_1^{(1)}} & \frac{\partial F_2}{\partial G_2^{(1)}} & \cdots & \frac{\partial F_2}{\partial G_n^{(1)}} \\ \vdots & \vdots & & \vdots & \vdots & \vdots & & \vdots \\ \frac{\partial F_{2n}}{\partial G_1} & \frac{\partial F_{2n}}{\partial G_2} & \cdots & \frac{\partial F_{2n}}{\partial G_n} & \frac{\partial F_{2n}}{\partial G_1^{(1)}} & \frac{\partial F_{2n}}{\partial G_2^{(1)}} & \cdots & \frac{\partial F_{2n}}{\partial G_n^{(1)}} \end{pmatrix}, \tag{4.57}$$

where

$$\begin{aligned} \frac{\partial F_2}{\partial G_\mu}(\rho, G_\nu) &= A_1^{(6)}\frac{\partial E_1}{\partial G_\mu} + A_{\mu 1}^{(3)} D_\mu E_1 + A_{\mu 1}^{(2)} E_\mu E_1 \\ &\quad + \sum_{\tau=1}^{n}\left(A_{\tau 1}^{(5)} + A_{\tau 1}^{(3)} G_\tau\right)\left(\frac{\partial D_\tau}{\partial G_\mu}E_1 + D_\tau\frac{\partial E_1}{\partial G_\mu}\right) \\ &\quad + \sum_{\tau=1}^{n}\left(A_{\tau 1}^{(4)} + A_{\tau 1}^{(2)} G_\tau + A_{\tau 1}^{(1)} G_\tau^{(1)}\right)\left(\frac{\partial E_\tau}{\partial G_\mu}E_1 + E_\tau\frac{\partial E_1}{\partial G_\mu}\right) \end{aligned} \tag{4.58}$$

and similar relations for $\frac{\partial F_2}{\partial G_\mu^{(1)}}$ and the partial derivatives of the other nonlinear functions $F_3, \ldots, F_{2n}$.

The partial derivatives $\frac{\partial D_\tau}{\partial G_\mu}$, $\frac{\partial E_\tau}{\partial G_\mu}$, $\frac{\partial D_\tau}{\partial G_\mu^{(1)}}$, and $\frac{\partial E_\tau}{\partial G_\mu^{(1)}}$ required in (4.58) are obtained by implicit differentiation of eqs. (4.34)

$$\begin{aligned} \sum_{\tau=1}^{n} O_{\nu\tau}\frac{\partial D_\tau}{\partial G_\mu} + \sum_{\tau=1}^{n} P_{\nu\tau}\frac{\partial E_\tau}{\partial G_\mu} &= \frac{\partial Q_\nu}{\partial G_\mu} - \sum_{\tau=1}^{n}\frac{\partial O_{\nu\tau}}{\partial G_\mu}D_\tau - \sum_{\tau=1}^{n}\frac{\partial P_{\nu\tau}}{\partial G_\mu}E_\tau \\ &= -\left(B_{\mu\nu}^{(3)} G_\nu + B_{\mu\nu}^{(6)}\right) D_\mu \\ &\quad -\left(B_{\mu\nu}^{(2)} G_\nu + B_{\mu\nu}^{(5)}\right) E_\mu \\ &\quad -\left\{\sum_{\tau=1}^{n}\left(B_{\tau\nu}^{(1)} G_\tau^{(1)} + B_{\tau\nu}^{(2)} G_\tau + B_{\tau\nu}^{(7)}\right) E_\tau \right. \end{aligned}$$

$$+\sum_{\tau=1}^{n}\left(B_{\tau\nu}^{(3)}G_\tau+B_{\tau\nu}^{(8)}\right)D_\tau+B_\nu^{(11)}\Bigg\}\delta_{\mu\nu}.$$

$$\sum_{\tau=1}^{n}O_{\nu\tau}\frac{\partial D_\tau}{\partial G_\mu^{(1)}}+\sum_{\tau=1}^{n}P_{\nu\tau}\frac{\partial E_\tau}{\partial G_\mu^{(1)}} = -\left(B_{\mu\nu}^{(1)}G_\nu+B_{\mu\nu}^{(4)}\right)E_\mu \tag{4.59}$$

and similarly for the second linear system (4.34). $\delta_{\mu\nu}$ denotes the Kronecker delta given by

$$\delta_{\mu\nu}=\begin{cases}1 & \text{for} \quad \mu=\nu\\ 0 & \text{otherwise}\end{cases}. \tag{4.60}$$

Solution of the nonlinear equations via the procedure described above yields the G_ν and $G_\nu^{(1)}$) as functions of ρ and u. We now calculate the derivatives $\frac{\partial G_\nu}{\partial u}(\rho,u)$ and $\frac{\partial G_\nu^{(1)}}{\partial u}(\rho,u)$ required in the coefficient $B(\rho,u)$ in eq. (4.44). They are determined by implicitly differentiating equations $F_1=0,\ldots,F_{2n}=0$ with respect to u

$$\begin{pmatrix}\frac{\partial G_1}{\partial u}\\ \frac{\partial G_2}{\partial u}\\ \vdots\\ \frac{\partial G_n}{\partial u}\\ \frac{\partial G_1^{(1)}}{\partial u}\\ \frac{\partial G_2^{(1)}}{\partial u}\\ \vdots\\ \frac{\partial G_n^{(1)}}{\partial u}\end{pmatrix}=J\left(\rho,G_\nu(\rho,u),G_\nu^{(1)}(\rho,u)\right)^{-1}\cdot\begin{pmatrix}-1\\ 0\\ \vdots\\ 0\end{pmatrix}. \tag{4.61}$$

Finally, the $\frac{\partial a}{\partial G_\nu}(\rho,u)$ and $\frac{\partial a}{\partial G_\nu^{(1)}}(\rho,u)$ are obtained from (4.36),

$$\begin{aligned}\frac{\partial a}{\partial G_\nu} &= A^0\frac{\partial M}{\partial G_\nu}-\frac{4}{\sigma^2}B^0\frac{\partial N}{\partial G_\nu}\\ \frac{\partial a}{\partial G_\nu^{(1)}} &= A^0\frac{\partial M}{\partial G_\nu^{(1)}}-\frac{4}{\sigma^2}B^0\frac{\partial N}{\partial G_\nu^{(1)}},\end{aligned} \tag{4.62}$$

where

$$\begin{aligned}\frac{\partial M}{\partial G_\nu} = -\rho\sum_{\tau=1}^{n}\Bigg[&\left(\frac{M_\tau^{(a)}}{z_\tau^2}-2\pi\rho\frac{G_\tau}{z_\tau^4}(M_\tau^{(a)}e^{-z_\tau\sigma}-1)\right)\frac{\partial D_\tau}{\partial G_\nu}\\ &+\left(\frac{P_\tau^{(a)}}{z_\tau^2}-2\pi\rho\frac{G_\tau}{z_\tau^4}(2L_\tau^{(a)}e^{-z_\tau\sigma}-2)-2\pi\rho\frac{G_\tau^{(1)}}{z_\tau^3}(M_\tau^{(a)}e^{-z_\tau\sigma}-1)\right)\frac{\partial E_\tau}{\partial G_\nu}\Bigg]\\ &+2\pi\rho^2\frac{1}{z_\nu^4}(M_\nu^{(a)}e^{-z_\nu\sigma}-1)+2\pi\rho^2\frac{1}{z_\nu^4}(2L_\nu^{(a)}e^{-z_\nu\sigma}-2)\end{aligned} \tag{4.63}$$

and similarly for $\frac{\partial M}{\partial G_\nu^{(1)}}$, $\frac{\partial N}{\partial G_\nu}$ and $\frac{\partial N}{\partial G_\nu^{(1)}}$ with $\{D_\mu,E_\mu,\frac{\partial D_\mu}{\partial G_\nu},\frac{\partial E_\mu}{\partial G_\nu},\frac{\partial D_\mu}{\partial G_\nu^{(1)}},\frac{\partial E_\mu}{\partial G_\nu^{(1)}}\}$ as functions of $(\rho,G_\nu(\rho,u),G_\nu^{(1)}(\rho,u))$.

The PDE (4.43) is a quasilinear diffusion equation that has been solved numerically by an implicit finite-difference algorithm [80] described in detail in [43] in the region $(\beta,\rho)\in[0,\beta_f]\times[0,\rho_0]$. The integration with respect to β starts at $\beta=0$ and goes down to lower temperatures. At each temperature the set of nonlinear equations (4.46), (4.54)-(4.56) is solved giving G_ν and $G_\nu^{(1)}(\rho,u)$: to ensure rapid convergence the values of the G_ν and $G_\nu^{(1)}(\rho,u)$ obtained at the previous temperature step in the solution algorithm of the PDE are taken as initial guess for the solution of the system of nonlinear equations. In the next step $\{D_\mu,E_\mu\}(\rho,u)$, $a(\rho,u)$, $\{\frac{\partial D_\mu}{\partial G_\nu},\frac{\partial E_\mu}{\partial G_\nu},\frac{\partial D_\mu}{\partial G_\nu^{(1)}},\frac{\partial E_\mu}{\partial G_\nu^{(1)}}\}(\rho,u)$, $\{\frac{\partial a}{\partial G_\nu},\frac{\partial a}{\partial G_\nu^{(1)}}\}(\rho,u)$, and $\{\frac{\partial G_\nu}{\partial u},\frac{\partial G_\nu^{(1)}}{\partial u}\}(\rho,u)$ are determined to calculate the coefficient $B(\rho,u)$.

The boundary conditions are the same as in [48]: for $\rho=0$ one obtains from eq. (4.38)

$$u(\rho=0,\beta)=0\quad\forall\beta. \tag{4.64}$$

For the boundary condition at high density ρ_0 (we have set $\rho_0^\star=\rho_0\sigma^3=1$ in the calculations) we make use of the so-called high temperature approximation

$$\frac{\partial^2 u}{\partial\rho^2}(\rho_0,\beta)=\frac{\partial^2 u}{\partial\rho^2}(\rho_0,\beta=0)\quad\forall\beta. \tag{4.65}$$

The initial condition $u(\rho,\beta=0)$ can be determined by taking into account that for $\beta=0$ the direct correlation function $c(r)$ coincides with that of the HS gas. Thus $\widetilde{K}_\nu=0$ for $\nu=2,\ldots,n$, $\tilde{L}_\nu=0$ for $\nu=1,\ldots,n$, yielding $D_\nu(\rho,\beta=0)=0$ for $\nu=2,\ldots,n$, and $E_\nu(\rho,\beta=0)=0$ for $\nu=1,\ldots,n$. Hence, the first system of linear equations (4.34) reduces to

$$O_{\nu 1}D_1=Q_\nu\quad\text{for}\quad\nu=1,\ldots,n. \tag{4.66}$$

For $\nu=1$ this leads to

$$D_1(\rho,\beta=0)=\frac{Q_1(G_1(\rho,\beta=0))}{O_{11}(G_1(\rho,\beta=0))}, \tag{4.67}$$

where $G_1(\rho,\beta=0)$ is obtained from the known quantity $\gamma_1(\rho,\beta=0)$ that was introduced in the Laplace transform technique (see Appendix A of [48]) via

$$G_1(\rho,\beta=0)=\frac{z_1}{4\pi\rho}\frac{A-1}{A\sigma_1-\tau_1}, \tag{4.68}$$

where

$$\begin{aligned}
A &= (2-\sqrt{q}-\gamma_1(\rho,\beta=0))\,\frac{2(2+z_1)}{4+2z_1-z_1^2}\\
\sigma_1 &= \frac{1}{2z_1}\left(\frac{z_1-2}{z_1+2}+e^{-z_1}\right)\\
\tau_1 &= \frac{1}{2z_1}\left(\frac{z_1^2+2z_1-4}{4+2z_1-z_1^2}+e^{-z_1}\right)\\
q &= \frac{(1+2\eta)^2}{(1-\eta)^2}
\end{aligned} \tag{4.69}$$

with $\eta = \frac{\pi}{6}\rho$ being the packing fraction. From eq. (4.66), for $\nu > 1$, one obtains

$$G_\nu(\rho, \beta = 0) = -\frac{D_1(\rho, \beta = 0)\left(B_{1\nu}^{(6)} G_1(\rho, \beta = 0) + B_{1\nu}^{(10)}\right) + B_\nu^{(12)}}{D_1(\rho, \beta = 0)\left(B_{1\nu}^{(3)} G_1(\rho, \beta = 0) + B_{1\nu}^{(8)}\right) + B_\nu^{(11)}}. \tag{4.70}$$

The second linear system (4.34) reduces to

$$R_{\nu 1} D_1 = T_\nu \quad \text{for} \quad \nu = 1, \ldots, n, \tag{4.71}$$

from which one can eliminate the $G_\nu^{(1)}(\rho, \beta = 0)$ once the $G_\nu(\rho, \beta = 0)$ are known

$$G_\nu^{(1)}(\rho, \beta = 0) = -\frac{D_1\left(D_{1\nu}^{(6)} G_1 G_\nu + D_{1\nu}^{(10)} G_\nu + D_{1\nu}^{(13)} G_1 + D_{1\nu}^{(15)}\right) + D_\nu^{(17)} G_\nu + D_\nu^{(18)}}{D_1\left(D_{1\nu}^{(3)} G_1 + D_{1\nu}^{(8)}\right) + D_\nu^{(16)}}. \tag{4.72}$$

Collecting these results one obtains

$$u(\rho, \beta = 0) = -2\pi\rho^2\epsilon\sigma \sum_{\nu=2}^{n} \left(\frac{K_\nu}{z_\nu} G_\nu(\rho, \beta = 0) + L_\nu G_\nu^{(1)}(\rho, \beta = 0)\right). \tag{4.73}$$

The unphysical region inside the spinodal curve is determined as follows: in the forbidden region either a eq. (4.36) becomes negative or no longer a solution of the system of the nonlinear equations (A.1), (A.2) can be found. The boundary conditions on the spinodal used here are the same as those in [48]

$$u(\rho_{S_i}, \beta) = u_S(\rho_{S_i}) \quad i = 1, 2, \tag{4.74}$$

where $\rho_{S_i} (i = 1, 2)$ are approximates for the spinodal densities on the discrete density grid at a given temperature. Their values are determined by locating the change of sign of a. $u_S(\rho)$ is the value of the excess internal energy per unit volume where $\frac{1}{\chi^{red}} = 0$. This value is determined by solving the set of equations

$$\begin{aligned} a(\rho, G_\nu, G_\nu^{(1)}) &= 0 \\ F_2(\rho, G_\nu, G_\nu^{(1)}) &= 0 \\ &\vdots \\ F_{2n}(\rho, G_\nu, G_\nu^{(1)}) &= 0 \end{aligned} \tag{4.75}$$

with respect to the G_ν and $G_\nu^{(1)}$, providing again the analytic Jacobian matrix of this nonlinear system. Inserting the solutions $G_\nu(\rho)$ and $G^{(1)}(\rho)$ in the energy equation (4.38) yields $u_S(\rho)$.

Once $u(\rho,\beta)$ has been determined by solving the PDE (4.43), the pressure P and the chemical potential μ are obtained by integrating $\frac{\partial\beta P}{\partial\beta}$ and $\frac{\partial\beta\mu}{\partial\beta}$ with respect to β from

$$\frac{\partial\beta P}{\partial\beta} = -u+\rho\frac{\partial u}{\partial\rho} \tag{4.76}$$

$$\frac{\partial\beta\mu}{\partial\beta} = \frac{\partial u}{\partial\rho}, \tag{4.77}$$

where we have taken as integration constants at $\beta=0$ the CS values for βP and $\beta\mu$

$$\begin{aligned}\beta P(\rho,\beta=0) &= \rho\frac{1+\eta+\eta^2-\eta^3}{(1-\eta)^3}\\ \beta\mu(\rho,\beta=0) &= \ln\rho+\frac{8\eta-9\eta^2-3\eta^3}{(1-\eta)^3}.\end{aligned} \tag{4.78}$$

Alternatively, βP and $\beta\mu$ can be obtained by integrating, respectively, $\frac{1}{\chi^{red}}$ and $\frac{1}{\rho\chi^{red}}$ with respect to the density from

$$\begin{aligned}\left(\frac{\partial\beta P}{\partial\rho}\right)_T &= \frac{1}{\chi^{red}}\\ \left(\frac{\partial\beta\mu}{\partial\rho}\right)_T &= \frac{1}{\rho\chi^{red}}.\end{aligned} \tag{4.79}$$

Both paths lead to the same thermodynamics due to the thermodynamic consistency enforced by eq. (4.25). However, the latter route has a serious drawback: in order to reach the high density branch of the subcritical isotherms, that is separated from the low-density branch by the spinodal, one has to circumvent the forbidden region via a path 'around' the coexistence curve.

4.4 Results

Using the formalism presented in the previous section we have investigated four systems - in the following labeled F0, F1, F2, and F3 whose parameters are summarized in table 4.1. For the interaction potential of F0 we have chosen $K_2=0$, i.e. we consider a simple exponential potential $w(r)=-\epsilon e^{-z_2(r-\sigma)}$ as shown in figure 4.1. The interaction potentials of F1-F3 correspond to one Sogami-Ise tail consisting of two competing terms: an attractive exponential and a repulsive Yukawa tail. Their parameters are listed in table 4.1. Varying the value of the ratio $-L_2z_2/K_2$ from 1.1 (F1) to 0.9 (F3) offers a systematic variation of the characteristic properties of the interaction potentials: the location of the minimum of $\phi(r)$ is shifted to larger r values and the contact-value of $\phi(r)$ at the HS diameter

system	K_2/n	$L_2 z_2/n$	z_2	n
F0	0	1	1.8	1
F1	-1	1.1	1.8	5.18787
F2	-1	1	1.8	7.19039
F3	-1	0.9	1.8	10.53148

Table 4.1: Parameters of the 4 SI systems investigated in this work. The normalization factors n were chosen so that the minimum of the function $w(r)$ of eq. (4.19) on the interval $[\sigma, \infty)$ is -1.

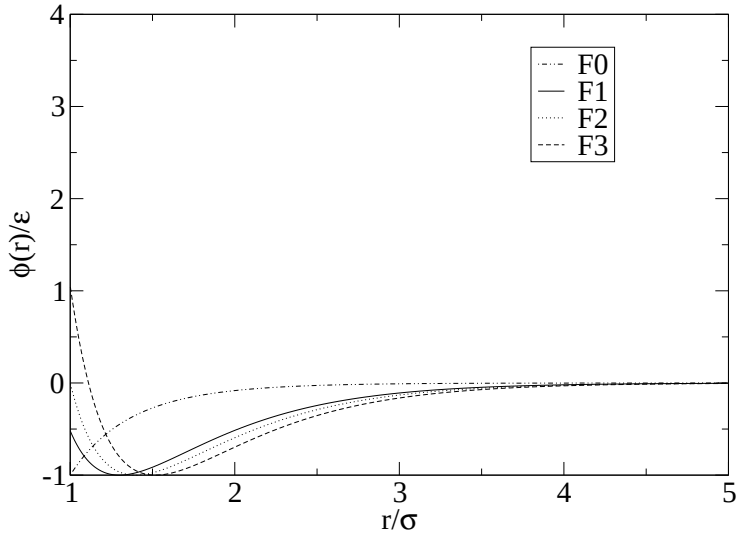

Figure 4.1: Sogami-Ise interaction potential of systems F0-F3. Parameters of the systems are given in table 4.1.

varies from negative to positive values as shown in figure 4.1. So for F3 a soft repulsive interaction merges into the infinitely steep repulsive HS wall.

For the 4 systems characterized above, we have calculated thermodynamic properties and the phase diagrams using the SCOZA as presented before; these results have been compared with results from the LOGA/ORPA approach [20, 21], according to which in equation (4.40) $K(\rho,\beta) = -\beta$ is fixed. This enables us to investigate the effect of self-consistency on the thermodynamic properties and on the phase behavior.

The LOGA/ORPA results have been obtained by solving the $4n$ equations (A.1)-(A.4) in the $4n$ unknowns $\{D_\nu, E_\nu, G_\nu, G_\nu^{(1)}\}$ with a Newton-Raphson technique providing a $4n \times 4n$ analytic Jacobian matrix. In the cases studied here, where the number of Sogami-Ise tails $n = 2$, the LOGA/ORPA values of $A_\nu^{(7)}$ and $C_\nu^{(13)}$ needed in eqs. (A.1) and (A.2) are given by $A_1^{(7)} = 0$, $C_1^{(13)} = 2\pi K_1(\rho)$, $A_2^{(7)} = 2\pi\beta\epsilon\sigma L_2$, and $C_2^{(13)} = 2\pi\beta\epsilon\sigma K_2$. Once the $\{D_\nu, E_\nu, G_\nu, G_\nu^{(1)}\}$ are known the excess internal energy via the internal energy route is calculated from eq. (4.38), the compressibility from eqs. (4.35)-(4.37), the pressure and the chemical potential via the energy route, P^E and μ^E, from eqs. (4.76) and (4.77), and the corresponding quantities via the compressibility route, P^C and μ^C, from eqs. (4.79).

Due to the inbuilt consistency SCOZA provides only two pressures in the following denoted as $P^{E,C}$ (via energy/compressibility route) and P^V (via the virial route). In SCOZA and LOGA/ORPA the virial pressure, P^V, has been obtained as described in detail in Appendix C.

In the following, fluid densities and temperatures are given in reduced units, i.e. $\rho^\star = \rho\sigma^3$, $T^\star = kT/\epsilon$. In figure 4.2 the pressure obtained from SCOZA via the energy/compressiblity route $P^{E,C}$ for system F2 is compared with the pressure calculated within LOGA/OPRA via the 3 different routes to thermodynamics. The LOGA/ORPA values for P^V and P^C bracket P^E (via LOGA/ORPA) which coincides - within the line thickness - with the SCOZA $P^{E,C}$. In table 4.2 the SCOZA predictions for the pressure and the chemical potential are compared with the LOGA/ORPA results for various thermodynamic states. For the slightly supercritical thermodynamic state of F0 at $\rho^\star = 0.3$ and $T^\star = 2$ (see figure 4.3) the agreement is less satisfactory than for the other non-critical states where the SCOZA and the LOGA/ORPA provide via the energy route results that are very close together. Within SCOZA discrepancies between pressure values $P^{E,C}$ and P^V are observed which are due to the fact that SCOZA in its present form enforces consistency only between the compressibility and the energy routes, and not with the virial route to thermodynamics. As becomes visible from table 4.2 SCOZA yields liquid-state pressures from the virial route that are very close to the results for the virial pressure within the LOGA/ORPA approach.

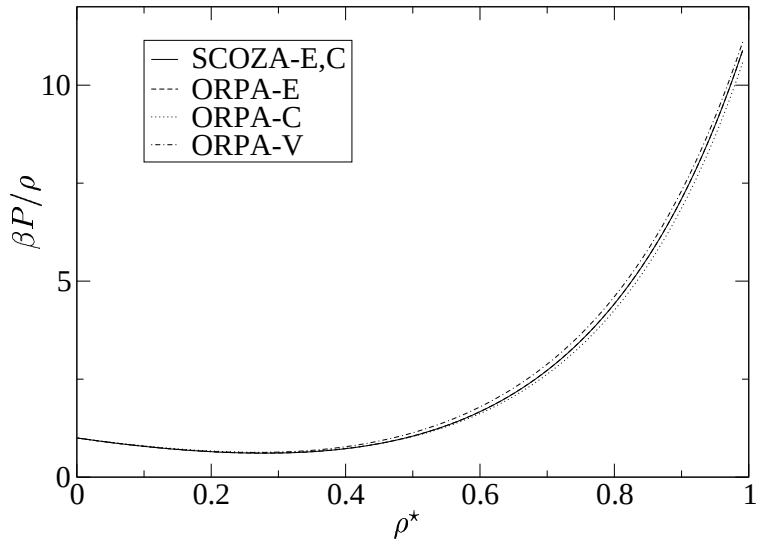

Figure 4.2: Pressure of system F2 at temperature $\beta^\star = 1/T^\star = 0.15$ obtained from SCOZA via energy/compressibility route and from LOGA/ORPA via energy, compressibility and virial route.

			SCOZA		LOGA/ORPA		
system	$\rho^\star$	$\beta^\star$	$\beta P^{E,C}/\rho$	$\beta P^V/\rho$	$\beta P^E/\rho$	$\beta P^C/\rho$	$\beta P^V/\rho$
F0	0.3	0.5	0.35744	0.25720	0.35492	0.46559	0.25094
F0	0.8	0.5	2.8874	2.7729	2.8872	3.2168	2.7703
F2	0.3	0.15	0.61502	0.63693	0.61500	0.63383	0.63750
F2	0.8	0.15	4.4201	0.46125	4.4214	4.2573	4.6053
system	$\rho^\star$	$\beta^\star$	$\beta\mu^{E,C}$		$\beta\mu^E$	$\beta\mu^C$	
F0	0.3	0.5	-2.6379		-2.6365	-2.4114	
F0	0.8	0.5	0.6155		0.61582	1.2652	
F2	0.3	0.15	-2.16945		-2.1690	-2.1124	
F2	0.8	0.15	3.0519		3.0543	2.8984	

Table 4.2: Pressure and chemical potential for systems F0 and F2 for selected thermodynamic states obtained from SCOZA and from LOGA/ORPA via the different routes.

Internal energy per particle via the energy route and reduced isothermal compressibility via the compressiblity route are compared in table 4.3. Again for the supercritical state at $\rho^\star = 0.3$ and $T^\star = 2$ of system F0 the results - especially of $1/\chi^{red}$ - differ.

			$U^{ex}/\epsilon N$		$1/\chi^{red}$	
system	$\rho^\star$	$\beta^\star$	SCOZA	LOGA/ORPA	SCOZA	LOGA/ORPA
F0	0.3	0.5	-3.2785	-3.2297	0.053807	0.27147
F0	0.8	0.5	-8.9067	-8.9062	17.028	17.611
F2	0.3	0.15	-9.1495	-9.1486	0.70248	0.71092
F2	0.8	0.15	-23.658	-23.659	21.332	20.617

Table 4.3: Reduced internal energy per particle and isothermal compressibility for systems F0 and F2 for selected thermodynamic states obtained from SCOZA and from LOGA/ORPA.

The phase diagram of the system F0 is given in figure 4.3. The SCOZA critical point has been located by the vanishing of $1/\chi^{red}$. Below $T_c^\star$ the spinodal line was determined as described in section 4.3. The coexistence curve was obtained by numerically solving the equilibrium conditions

$$\mu(\rho_g, T) = \mu(\rho_l, T) \tag{4.80}$$

$$P(\rho_g, T) = P(\rho_l, T) \tag{4.81}$$

for the two coexisting densities ρ_g and ρ_l of the gas and liquid for a given temperature T. While the coexistence curve of the SCOZA can be determined up to the critical point, this is not possible for the LOGA/ORPA: near the critical point no solution of eqs. (4.80) and (4.81) can be found so the two branches remain unconnected. Therefore the critical point parameters $\rho_c^\star$ and $T_c^\star$ within the LOGA/ORPA, collected in table 4.4, were obtained by extrapolation under the assumption that the coexistence curve can be described by a scaling type law and the law of rectilinear diameters, i.e.

$$\rho_l - \rho_g = B(T - T_c)^\beta \qquad (\rho_l + \rho_g)/2 = \rho_c + A(T - T_c) \tag{4.82}$$

Parameters A,B, and β in eqs. (4.82) were fitted to the coexistence curves.

In figure 4.3 also the inconsistency of the LOGA/ORPA becomes visible: the curve of diverging compressibility falls well inside the liquid-vapor coexistence curve obtained from the energy route yielding two different critical points. The SCOZA value is closer to the one derived from the energy route which is known to yield the most accurate thermodynamic information from the radial distribution function within the LOGA/ORPA approach.